The calcium binding protein S100β marks Hedgehog-responsive perivascular stem cells that contribute to intimal thickening following iatrogenic flow restriction

¶Mariana Di Luca[1], ¶Emma Fitzpatrick[1], ¶Denise Burtenshaw[1], ¶Weimin Liu[2], Jay-Christian Helt[2], Roya Hakimjavadi[1], Eoin Corcoran[1], Yusof Gusti[1], Daniel Sheridan[1], Susan Harman[1], Catriona Lally[3], Eileen M. Redmond[2] and Paul A. Cahill*[1]

[1] Dublin City University, Vascular Biology & Therapeutics Group, School of Biotechnology (Dublin, Ireland); [2] University of Rochester, Dept Surgery (Rochester, New York, United States) [3]Trinity College Dublin, Trinity Centre for Bioengineering, Trinity Biomedical Sciences Institute, (Dublin, Ireland).

¶ Contributed equally

*Address for correspondence

Paul A. Cahill., BSc., PhD
Professor, School of Biotechnology
Chair of Vascular Biology & Therapeutics, School of Biotechnology
Lonsdale Bldg, Office X2-09, Faculty of Science and Health
Dublin City University, Glasnevin, Dublin 9. Ireland
E: paul.cahill@dcu.ie, Ph: 353-1-700-8466, Fax: 353-1-700-5412

Summary

A hallmark of subclinical atherosclerosis is the accumulation of vascular smooth muscle cell (SMC)-like cells leading to intimal thickening. While medial SMCs contribute, the participation of hedgehog responsive resident vascular stem cells (vSCs) to lesion formation remains unclear. Using transgenic eGFP mice and genetic lineage tracing of S100β vSCs *in vivo*, we identified S100β/Sca1 cells derived from a perivascular S100β non-SMC parent population within lesions following iatrogenic flow restriction, an effect attenuated following hedgehog inhibition with cyclopamine. Multipotent S100β/Sca1 vSCs acquired the stable SMC epigenetic H3K4me2 histone mark at the Myh11 locus and underwent myogenic differentiation in response to sonic hedgehog (SHh) *in vitro.* S100β cells were enriched in human arteriosclerotic lesions while SHh promoted myogenic differentiation of human induced pluripotent stem cell derived S100β neuroectoderm progenitors *in vitro.* We conclude that hedgehog responsive S100β vSCs contribute to lesion formation and support targeting hedgehog signalling to treat subclinical arteriosclerosis.

Keywords: Arteriosclerosis, intimal thickening, resident vascular stem cells, S100β calcium binding proteins, stem cell antigen-1, lineage tracing, hedgehog signalling, human induced pluripotent stem cells (HiPSCs).

Introduction

Atherosclerosis is a chronic progressive inflammatory disease that leads to myocardial infarction and stroke (Bennett et al., 2016). Pathologic observations in humans vessels confirm that early 'transitional' lesions enriched with smooth muscle (SMC)-like cells called adaptive lesions are routinely present in atherosclerotic-prone regions of arteries before pathologic intimal thickening, lipid retention, and the appearance of a developed plaque (Sakamoto et al., 2018). Endothelial cell (EC) dysfunction due to disturbed blood flow is classically associated with the development of atheroprone lesions (Halcox et al., 2009; Hromada et al., 2017; Zhang et al., 2013), while the embryological origin (e.g., neuroectoderm versus mesoderm) of SMCs may also influence disease localisation and progression (Sinha et al., 2014). These early lesions are routinely modelled in mouse carotid arteries following flow restriction (Korshunov and Berk, 2003) and can further rapidly develop into advanced atherosclerotic plaques in ApoE knockout on a Western diet (Liu et al., 2011; Nam et al., 2009).

Lineage tracing and single cell RNA sequence analysis (scRNA-seq) have provided compelling evidence in various animal models for the involvement of a rare population of (i) differentiated myosin heavy chain 11 (Myh11) medial SMC that are stem cell antigen-1 (Sca1) (Chappell et al., 2016; Dobnikar et al., 2018) and (ii) various adventitial and medial progenitors in progressing intimal thickening (Kramann et al., 2016; Tang et al., 2020, 2012; Yuan et al., 2017). While some adventitial progenitors are derived from a parent Myh11 SMC population (Majesky et al., 2017), non-SMC derived SRY-related HMG-box 10 (Sox10) adventitial/medial resident multipotent vascular stem cells (vSC), glioma-associated oncogene homolog 1 (Gli) and Nestin progenitor cells have also been implicated (Kramann et al., 2016; Wan et al., 2012). Despite these insights, the putative role of resident vSCs that do not originate from medial Myh11 SMCs in promoting intimal thickening remains controversial.

S100β, a member of the S100 multigenic family expressing small (9 kDa and 14 kDa) Ca2+-binding proteins of the EF-hand type, is primarily localised to astrocytes and glial cells under normal physiological conditions and is positively associated with age and various neurodegenerative and neuroinflammatory diseases (Donato et al., 2009). S100β promotes intimal thickening through interaction with the receptor for advanced glycation end-products (RAGE) (Cao et al., 2017) and induces migration and infiltration of inflammatory cells (Sagheddu et al., 2018; Zhou et al., 2018). S100β plays a crucial role in maintaining an intermediate state

of Sca1 progenitor cells following injury-induced neointimal thickening through a RAGE and stromal cell-derived factor-1 α/CXCR4 signalling mechanism (Wu et al., 2019).

Hedgehog signalling (Hh) is essential for normal embryonic development (Ingham and McMahon, 2001) and plays a pivotal role in the maintenance of adult progenitor/stem cells in tissue repair after injury (Petrova and Joyner, 2014). Hh signalling is initiated upon binding of a ligand to the canonical receptors, PTCH1 and PTCH2 (Patched 1 and 2) (Marigo et al., 1996a), which leads to disinhibition of SMO (Smoothened) and activation a complex signalling cascade that regulates the GLI (glioma-associated oncogene homolog 1) family zinc finger transcription factors (GLI1, GLI2, and GLI3) (Briscoe and Thérond, 2013). GLI activators induce the transcription of Hh target genes primarily involved in cell proliferation, cell survival, and cell fate specification, including PTCH and GLI (Marigo and Tabin, 1996; Marigo et al., 1996b) . HHIP (hedgehog interacting protein) modulates hedgehog signalling activity by binding and inhibiting the action of hedgehog proteins (Chuang and McMahon, 1999). Genome wide association studies (GWAS) in coronary artery disease patients have since identified variants at the 14q32 HHIPL1 (Hedgehog interacting protein-like 1) that encode a paralog of HHIP (López-Mejías et al., 2017) to increase Hh signalling and regulate SMC proliferation and migration *in vitro* (Aravani et al., 2019). In atherosclerotic mice, Hh has a permissive role through increased lipid uptake by macrophages (Beckers et al., 2007), while global Hhipl1 deletion reduces plaque burden (Aravani et al., 2019). Hh signalling, especially SHh and signal peptide CUB domain and EGF like domain containing 2 (Scube2), are overexpressed in injured arteries during lesion formation after flow restriction (Ali et al., 2013; Dutzmann et al., 2017; Morrow et al., 2009), autogenous vein grafts (Li et al., 2010), and hypoxic pulmonary arterial SMCs (Wang et al., 2010). Adventitial Sca1 that co-localise with SHh and Ptch1 (Passman et al., 2008) significantly contribute to intimal thickening *in vivo* (Dutzmann et al., 2017; Shikatani et al., 2016; Tsai et al., 2012) while Hh inhibition with cyclopamine or local perivascular depletion of Ptch1 attenuates intimal thickening following iatrogenic flow-restriction *in vivo* (Fitzpatrick et al., 2017; Redmond et al., 2013).

Given the pivotal role of Hh in the maintenance of adult progenitor/stem cells, tissue repair and atherosclerosis (Aravani et al., 2019; Petrova and Joyner, 2014), we sought to determine the role of Hh responsive S100β/Sca1 vSCs and their myogenic progeny in contributing to intimal thickening and the progression of adaptive lesions *in vivo* and, furthermore, whether

Hh signalling directs murine S100β vSCs and hiPSC-derived S100β neuroectoderm stem cells to undergo proliferation and myogenic differentiation *in vitro*.

Results

Perivascular Sca1 and S100β stem vSCs are present in normal adult vessels

The presence of perivascular Sca1 and S100β vSCs was first confirmed in whole mounted vessels from Sca1-eGFP and S100β-eGFP mice (Hayashi et al., 2007; Ma et al., 2002a). A discrete number of Sca1-eGFP and S100β-eGFP cells were present on collagen fibres within the adventitial layer of the thoracic aorta, when compared to wild-type (WT) controls [Suppl Figure 1A-D]. The cells were located predominantly at the aortic arch and at bifurcations with intercostal vessels, and their presence diminished along the descending and abdominal aorta [Suppl Figure 1B]. When the media was removed, Sca1-eGFP cells were clearly present in adventitial layer of the thoracic aorta [Suppl Figure 1D] and in perivascular regions of the carotid artery [Suppl Figure 1D].

Sca1 and S100β cells are present in intimal lesions from murine carotid arteries following iatrogenic flow restriction.

The contribution of Sca1 cells to intimal medial thickening following iatrogenic flow restriction was assessed in Sca1-eGFP transgenic mice following partial ligation of the left carotid artery (LCA). Vessels were harvested on day 3, 7 and 14 days post-ligation and paraformaldehyde fixed and paraffin-embedded cross sections were evaluated for eGFP (indicative of Sca1 expression) by confocal microscopy. Morphometric analysis confirmed that adventitial and intimal volumes increased significantly over time following ligation, without any significant change to medial volume, concomitant with a significant reduction in luminal volume after 7 and 14 days [Figure 1A].

The number of cells within the adventitial, medial and intimal layers of the LCA did not significantly change 3d post ligation [Figure 1B-D]. No Sca1- eGFP cells were visible within the medial layer of sham vessels which was populated primarily by α-smooth muscle actin (SMA)

SMCs [Figure 1E]. While a small but significant number of Sca1-eGFP cells were present within the adventitial and intimal layers of sham vessels [Figure 1E, F], the fraction of Sca1-eGFP cells significantly increased within the intimal layer 3d post ligation [Figure 1E, F]. Immunohistochemical analysis using anti-eGFP confirmed the presence of intimal Sca1-eGFP cells in ligated vessels [Figure 1E] and further demonstrated that intimal Sca1-GFP cells co-express PECAM-1/CD31 and endothelial cell nitric oxide (eNOS) [Figure 1E]. There was also a notable increase in the expression of the pro-apoptotic protein, Bax (Pawlowski and Kraft, 2000) within the intimal, adventitial and medial layer of the LCA and the medial layer of the RCA 3d post ligation [Figure 1F, G], as previously described (Heo et al., 2011).

The presence of Sca1-eGFP cells within the neointimal layers was also observed after 7 and 14d ligation [Figure 2A, B] concomitant with an increase in the number of cells [Figure 2C,D] and volume of the neointimal layer [Figure 1A]. Cumulative analysis revealed that there was a significant increase in the fraction of Sca1-eGFP cells within neointimal layers after 7 and 14d [Figure 1E, F].

The contribution of S100β vSC to intimal medial thickening following iatrogenic flow restriction was also assessed in S100β-eGFP transgenic mice following ligation of the left carotid artery (LCA) for 21 d. S100β-eGFP cells were present within the adventitial layer of sham and the contralateral RCA and within the neointimal layer after 21d ligation [Figure 2G] and co-localised with Sca1 cells [Figure 2H]. Both Sca1 and S100β cells co-localised with SMA neointimal cells in ligated vessels [Figure I, J]. Cumulative analysis revealed that the fraction of S100β cells significantly increased within the medial and neointimal layers of ligated vessels compared to sham and the contralateral RCA [Figure 2K, L]. Similarly, the number of double positive Sca1/S100β cells significantly increased within the medial and neointimal layers of ligated vessels compared to the contralateral RCA [Figure 2M].

Lineage tracing analysis of marked perivascular S100β cells iatrogenic flow restriction.

In order to determine the source of medial and intimal Sca1/S100β cells following flow restriction, lineage tracing analysis was performed using transgenic S100β-eGFP-CreERT2-Rosa-26-tdTomato reporter mice [Suppl Figure 2A]. As cre-mediated recombination results in a permanent heritable change in a cell's genome, these cells and their progeny remain tdTomato (tdT) positive. The animals were treated with tamoxifen (Tm) for 7 days to induce nuclear

translocation of CreER(Tm) and subsequent recombination to indelibly mark S100β cells with red fluorescent tdT seven days before ligation was performed [Suppl Figure 2B]. Only S100β cells present during the period of Tm treatment and their subsequent progeny following injury are marked with tdT. The tissue specificity and recombination efficiency of the Tm-induced Cre activity was confirmed in bone-marrow smears and neuronal tissue from S100β-eGFP-CreERT2-Rosa-26-tdTomato mice. Treatment with Tm resulted in Cre-mediated recombination and expression of S100β- tdT in >90% of neuronal cells of the carotid sinus nerve (Hering's nerve) without any S100β-tdT cells observed in the bone marrow smears [Suppl Figure 2C]. The neuronal staining was confirmed by immunohistochemical analysis of S100β expression using both anti-S100β and anti-tdT antibodies (data not shown).

Morphometric analysis of the S100β-eGFP-creER2-Rosa26-tdT mice confirmed significant intimal thickening in transgenic mice following ligation injury when compared to the sham LCA and contralateral RCA [Figure 3A-C]. Treatment of S100β-eGFP-creER2-Rosa26-tdT transgenic mice with tamoxifen indelibly marked S100β cells (S100β-tdT) within the adventitial layer of the sham LCA prior to flow restriction [Figure 3D]. No cells are marked when these double transgenic mice were treated with the vehicle control (corn oil) [Figure 3D]. Importantly, no S100β-tdT cells were observed in the intimal (EC) or medial (SMC) layers of these sham vessels following tamoxifen treatment [Figure 3D]. However, following ligation, there was a striking increase in the number of S100β-tdT marked cells within the medial and intimal layers of the ligated LCA, compared to sham controls [Figure 3E, F]. In order to rule out the possibility that Tm treatment continues to label a significant number of cells for weeks after last Tm treatment (Reinert et al., 2012), we confirmed that the fraction of S100β-tdT marked cells remained significantly higher in the neointima of LCA four weeks after the last Tm injection when compared to the RCA [Suppl Figure 2D, E]. Moreover, the fraction of S100β-tdT marked cells within the LCA adventitial, medial and intimal layers of ligated vessels after one and four weeks from the last Tm injection was of a similar magnitude [Suppl Figure 2F].

When S100β-tdT marked cells were evaluated for co-expression of Sca1 by immunohistochemistry using anti-Sca1 and anti-tdT antibodies, there was a significant increase in the number of Sca1/S100β-tdT cells in all compartments of the LCA compared to the contralateral RCA [Figure 3G]. Cumulative analysis confirmed both a significant increase in the fraction of S100β-tdT cells [Figure 3H] and the fraction of double stained S100β/Sca1 cells

[Figure 3I] within the LCA medial and intimal layers compared to the contralateral RCA control. Moreover, the majority of Sca1 cells within ligated vessels were S100β-tdT cells [Figure 3J]. Since intimal and medial cells are not marked with tdT prior to injury, these data suggest that these cells are derived from a non-SMC S100β parent population following flow restriction. Moreover, the majority of intimal Sca1 cells are derived from an S100β parent population.

Hedgehog signalling components control intimal thickening following iatrogenic flow restriction

The effect of systemic administration of the Hedgehog inhibitor cyclopamine (10 mg/kg, IP, every other day) on neointimal thickening and the accumulation of Sca1-eGFP cells was evaluated. 2-hydroxypropyl-β-cyclodextrin (HβCD) was used as a vehicle control. Vessels were harvested 7 and 14 d post-ligation and morphometric analysis was performed. Whole vessel *Gli2* mRNA levels were significantly elevated in ligated vessels treated with HβCD when compared to sham controls (8.1 ± 0.9 fold, $p \leq 0.05$ n=4), an effect that was significantly reduced following cyclopamine treatment (3.2 ± 0.3 fold, n=4, $p \leq 0.05$). Immunohistochemical analysis revealed that the Hh receptor, Ptch1, was up-regulated in LCA following injury concomitant with enhanced Gli2 expression in LCA when compared to sham vessels [Figure 4A]. Gli2 co-localised with Sca1-eGFP expressing cells and was markedly increased in ligated vessels treated with vehicle (HβCD) when compared to sham-operated vessels, especially in the neointima and media of the LCA [Figure 4A], an effect that was attenuated following Hh inhibition [Figure 4A]. Cyclopamine treatment significantly reduced the fraction of Sca1-eGFP expressing cells [Figure 4B, C] concomitant with reduced intimal thickening 7 d and 14 d-post ligation [Figure 4D-G]. Collectively, these data suggest that intimal thickening is attenuated by systemic administration of the smoothened inhibitor, cyclopamine, concomitant with a reduction in the accumulation of Gli2/Sca1 Hh-responsive cells within the intimal and medial layers.

Isolation and characterisation of resident S100β/Sca1 vascular stem cells from murine aorta.

The expression of SMC differentiation markers genes, *Myh11* and *Cnn1* was enriched in medial segments from both atheroprone aortic arch (AA) and atheroresistant thoracic/abdominal aorta (TA) regions of the mouse aorta, when compared to NE-4C cells and immortalised MOVAS mSMCs in culture [Figure 5A]. The level of S100β and Sox10 expression, both markers of resident vascular stem cells (Kennedy et al., 2014; Tang et al., 2012), was then assessed in AA

and TA regions, with or without the adventitia [Figure 5B, C]. There was significant enrichment of both S100β and Sox10 in the AA when compared to the TA. Moreover, the levels were significantly enriched within the adventitia since its removal resulted in a dramatic reduction in the expression of both transcripts. Nevertheless, medial expression of both genes was still observed in the AA region [Figure 5B, C].

Resident vascular stem cells (vSCs) were subsequently isolated from mouse aortic arch (AA) and thoracic aorta (TA) by enzymatic digestion and sequential plating, and were characterised by immunocytochemistry, flow cytometry, and gene expression for both stem cell markers and SMC differentiation markers. Immunocytochemical analysis revealed that vSCs from both AA and TA regions were Sca1 positive and expressed neuroectodermal markers S100β, Sox10, Sox17, and Nestin but were negative for SMC differentiation markers *Cnn1* and *Myh11* [Figure 5D]. Flow cytometric analysis confirmed that the cells were Sca1 and S100β positive when compared to Sca1 and S100β positive control cell lines (i.e., C3H 10T1/2 and NE-4C, respectively) [Figure 5E]. The vSCs did not enrich for *Myh11* or *Cnn1* transcripts when compared to fresh aortic tissue [Figure 5F, G] but exhibited greater teleomere length as a measure of stemness when compared to freshly isolated aortic SMC and to the immortalised MOVAS SMCs in culture [Figure 5H]. The vSCs were enriched for neuroectodermal marker genes *S100β, Sox10 and Nestin* [Suppl Figure 3A-C], but not for mesoderm markers *Kdr, Pax1 and Tbx6* [Suppl Figure 3D-F], when compared to SMCs and NE-4 cells in culture. Collectively, these data indicate that neuroectodermal S100β/Sca1 cells are primarily located within the adventitial perivascular region of atheroprone regions of the mouse aorta and can be isolated and expanded *in vitro* to retain these phenotypic markers.

Hedgehog signalling promotes myogenic differentiation of resident murine S100β/Sca1 vascular stem cells *in vitro.*

The functional effect of sonic hedgehog (SHh) signalling on myogenic differentiation of vSCs was evaluated *in vitro* using multipotent Sca1/S100β cells isolated from mouse aorta. Treatment of vSCs isolated from AA and TA with recombinant SHh (rSHh, 0.5 µg/ml, 24h) promoted Hh signalling by increasing *Gli1* target gene mRNA levels, an effect blocked following pre-treatment with cyclopamine [Figure 5I, J]. Concurrent treatment of cells with rSHh for 7 days resulted in a significant increase in SMC differentiation marker (*Cnn1* and *Myh11*) mRNA levels, an effect attenuated by cyclopamine [Figure 5 I, J]. The level of enrichment of the SMC

specific epigenetic histone mark, di-methylation of lysine 4 on histone H3 (H3K4me2) and the repressor mark, tri-methylation of lysine 27 on histone H3 (H3K27me3) at the *Myh11* locus were both assessed using chromatin immunoprecipitation (ChIP) assays before and after rSHh treatment. Freshly isolated differentiated aortic medial SMC and murine embryonic stem cells (mESCs) were used as positive/negative controls for each mark and were markedly enriched for H3K4me2 and H3K27me3 at the Myh11 promoter, respectively [Figure 5K, M]. In contrast to medial SMCs, AA vSCs were enriched for H3K27me3 but lacked enrichment of H3K4me2 at this locus [Figure 5K, M]. Treatment with recombinant SHh (rSHh, 0.5 µg/ml, 7d) increased the enrichment levels of the H3K4me2 mark while concurrently decreasing the enrichment of the H3K27me3 mark, an effect attenuated by cyclopamine [Figure 5K-M]. Finally, SHh treatment significantly increased the fraction of $Cnn1^+$ and $Myh11^+$ cells in AA vSCs, an effect attenuated by pre-treatment with cyclopamine [Figure 5N, O].

S100β cells populate human arteriosclerotic lesions

The expression of S100β and the hedgehog receptor, PTCH1, was determined by immunofluorescence staining in normal and arteriosclerotic human aortic sections. The expression of SMA was abundant in the medial layers of both normal and arteriosclerotic vessels while reduced within the neointima [Figure 6A]. The expression of S100β was confined to the adventitial layer of normal vessels but was significantly enhanced within the adventitial and intimal layers of arteriosclerotic sections [Figure 6A]. The expression of PTCH1 was confined to the adventitial layers of normal vessels but was also sparsely expressed in the medial and intimal layers of arteriosclerotic sections [Figure 6A].

Hedgehog signalling promotes myogenic differentiation of human induced pluripotent stem cell (HiPSC)-derived neuroectodermal S100β vascular stem cells *in vitro.*

To address whether human neuroectoderm S100β progenitors (NEPs) respond to hSHh by undergoing myogenic differentiation, S100β NEPs were isolated from human induced pluripotent stem cells (HiPSC) using a chemically defined protocol (Cheung et al., 2012). Human iPSCs enriched for Oct4 were treated with neuroectodermal inductive stimuli (FGF-2 and the selective inhibitor of ALK5, SB413642) for 7 days [Figure 6B] and expressed S100β but not SMC differentiation markers CNN1 and MYH11 [Figure 6B]. Treatment of NEPs with myogenic media supplemented with TGF-β1/PDGF-BB significantly increases the fraction of CNN1 and MYH11

cells after a further 12 d in culture, while concomitantly decreasing the number of S100β cells [Figure 6C]. The levels of S100β, CNN1 and MYH11 transcripts mirrored the changes in protein, where NEP-derived SMCs became significantly enriched for CNN1 and MYH11 following TGF-β1/PDGF-BB treatment as they diminish their expression of S100β [Figure 6D-F]. Treatment of NEPs with rSHh (1.0 µg/ml) for 12 d resulted in a significant increase in CNN1 and MYH11 mRNA levels, an effect attenuated by cyclopamine [Figure 6G, H], concomitant with an increase in the number of CNN1 positive cells [Figure 6I].

Discussion

A hallmark of subclinical atherosclerosis is the accumulation of vascular smooth muscle cell (SMC)-like cells leading to intimal thickening (Shi et al., 2019). Endothelial dysfunction due to changes in blood flow and shear stress precedes the appearance of these lesions and is considered a pivotal event in the development of arteriosclerosis and subclinical atherosclerosis (Sakamoto et al., 2018). GWAS studies have linked exaggerated Hh signalling to SMC fate and atherosclerosis (Aravani et al., 2019). In this study, we used transgenic mice and genetic lineage tracing approaches to delineate the involvement of Hh responsive S100β resident VSCs in progressing neointima formation following flow restriction. Our findings indicate that intimal thickening involves significant accumulation of Hh-responsive perivascular S100β-derived progeny. Elucidation of this new cellular S100β source for generating SMC-like cells following injury expands our current understanding of vascular pathology and may represent an important therapeutic strategy for combating subclinical atherosclerosis.

SMC-like cells within neointimal lesions reportedly are monoclonal/oligoclonal in origin and arise from the expansion of a pre-existing resident clonal population of cells (Basatemur et al., 2019; Gomez and Owens, 2016; Hoglund et al., 2010; Murry et al., 1997). Despite extensive research, their origin has remained controversial (Nguyen et al., 2013). As a general rule, SMCs are purported to switch from a contractile phenotype to a less mature synthetic phenotype following vascular injury resulting in the loss of expression of SMC differentiation contractile markers, increased proliferation, and the synthesis and release of pro-inflammatory cytokines, chemotaxis-associated molecules and growth factors (Campbell and Campbell, 2012). However, whether these clonal progeny within lesions are derived primarily from differentiated medial SMCs (Campbell and Campbell, 2012; Chappell et al., 2016; Dobnikar et al., 2018), endothelial cells (Cooley et al., 2014; Yuan et al., 2017), and/or resident vSCs (Baker and Péault, 2016; Tang et al., 2020, 2012; Yuan et al., 2017; Zhang et al., 2018) remains unclear. Over the last decade, vascular SMC lineage tracing studies have provided compelling evidence of a significant role for pre-existing medial SMCs in vascular pathologies (Chappell et al., 2016; Herring et al., 2014; Nemenoff et al., 2011; Shankman et al., 2015). Single cell RNA sequence analysis (scRNA-seq) further identified a rare Sca1 Myh11-Cre marked SMC subpopulation that gives rise to functionally distinct neointimal cells during lesion progression in mice (Chappell et al., 2016; Dobnikar et al., 2018). However, although the Myh11-CreERT2 transgene was

originally deemed specific for vascular SMC (Owens, 2007), data indicating expression of this and other 'SMC differentiation genes' in non-SMC populations has recently emerged raising the possibility that other resident cells may contribute to lesion formation (Chakraborty et al., 2019; Murgai et al., 2017; Sheikh et al., 2014). Myh11-CreER SMC lineage tracing studies have also demonstrated that the fraction of SMCs originating from pre-existing SMCs may be considerably smaller after severe transmural injury in mice suggesting a contributory role for cells other than medial SMCs (Roostalu et al., 2018).

In this study, we provide genetic evidence that vascular lesions contain an abundance of dual S100β/Sca1 vSCs derived from a non-SMC perivascular S100β parent population following flow restriction. Notwithstanding the fact that Sca1 cells are present in bone-marrow (Tobin et al., 2017), bone-marrow cells were not marked using the S100β-CreERT2-tdT. As the majority of neointimal Sca1 cells were marked with S100β-Cre-tdT, it is most likely that the Sca1-eGFP cells observed within intimal lesions were locally derived (Hoglund et al., 2010). S100β-eGFP cells predominate within the adventitial layer of healthy vessels (murine and human) since removal of the adventitia dramatically reduced aortic S100β transcript levels in mice. However, we cannot rule out the presence of a rare plastic S100β cell within the adventitial-medial boundary since S100β cells were also successfully isolated from aortic medial segments following enzymatic digestion and sequential plating *in vitro*. Indeed, *in situ* histochemical analysis confirms the presence of a rare Sox10/S100β cell population within aortic media, in addition to the adventitia (Tang et al., 2013). Furthermore, a discrete population of immature medial cells expressing CD146 is also known to emerge during embryonic development and contribute to neointimal formation in response to injury (Roostalu et al., 2018). Whether these CD146 immature SMC progenitors are also S100β/Sca1 remains unclear although S100β vSCs derived from rat and murine aortic explants express CD146 (Kennedy et al., 2014; Tang et al., 2012). In the future, it will be important to determine whether medial S100β vSCs differ from CD146 (Roostalu et al., 2018) and Myh11-CreER Sca1 cells (Dobnikar et al., 2018) in their propensity to modulate different phenotypes and undergo clonal expansion using various injury models.

Adventitial progenitors have long been implicated in the progression of neointimal lesions following various vascular injuries (Hu et al., 2004; Psaltis et al., 2014; Shikatani et al., 2016). However, in the absence of Sca1 or c-kit$^+$ stem cell lineage tracing experiments *in vivo*, the hypothesis of a regenerative function for adventitial Sca1 or c-kit$^+$ vSCs in lesion formation has

been difficult to prove until recently. While perivascular cells must first traverse the internal and external elastic lamina to accumulate within the intima following injury (Wang et al., 2012), disruption of the elastic lamellae and flow-dependent enlargement of fenestrae can facilitate such migration (Campbell and Roach; Guo et al., 2008; Wong and Langille, 1996). Cell fate mapping studies have now clarified the role for adventitial PDGFRa Sca1 progenitors in lesion progression following severe injury (Tang et al., 2020) while c-kit progenitors minimally facilitate endothelial regeneration or SMC differentiation to SMCs (Chen et al., 2018). As Sca1-CreER marked cells were not present in vascular lesions following wire-induced injury (Tang et al., 2020), the origin of Sca1 neointimal cells following flow restriction in the current study is unlikely to be from a Sca1 parent population despite expressing Sca1 (albeit using a different injury model). Indeed, the percentage of perivascular S100β-CreER marked cells that were $Sca1^{pos}$ in normal vessels was < 50% indicating that a $Sca1^{neg}/S100\beta^{pos}$ population might be responsible. In this context, S100β has been shown to maintain an intermediate state of Sca1 progenitor cells following lesion formation (Wu et al., 2019). Alternatively, this residual $Sca1^{neg}/S100\beta^{pos}$ population of adventitial Sca1 cells might represent Sca1 cells derived from differentiated Myh11-CreER SMCs that expand in number following injury and contribute to adventitial remodelling (Majesky et al., 2017) and lesion formation (Dobnikar et al., 2018). While Sca1/S100β cells were predominantly found in the developing intimal layer after 7, 14 and 21 days, these cells were also present in the medial layer following injury. In agreement with previous studies demonstrating significant apoptosis of medial SMCs following flow restriction (Skelly et al., 2007), the appearance of medial Sca1/S100β cells marked with S100β-CreERT2-tdT following early expression of the pro-apoptotic protein Bax within the media is consistent with regeneration of medial SMCs following injury.

Previous lineage tracing studies have also implicated endothelial cells (EC) that undergo endothelial-to-mesenchymal transition (EndMT) to SMC-like cells as contributing to neointimal formation during vein graft remodelling (Cooley et al., 2014; Yuan et al., 2017). EndMT promotes neointimal hyperplasia and induces atherogenic differentiation of EC (Moonen et al., 2015). In the current study, EC were not marked with S100β-CreERT2-tdT prior to flow restriction suggesting that the S100β-CreERT2-tdT marked cells within lesions do not originate from an EC parent population. These apparent differences may result from the use of different models of vascular injury where vein graft and atherosclerosis models involve different

biomechanical stimuli and/or a different inflammatory environments compared to the flow restriction model (Cooley et al., 2014; Souilhol et al., 2018). While EC did not contribute to neointimal formation in developed lesions, a potential role for adluminal Sca1 cells in regenerating the endothelium following ligation was observed. As flow restriction leading to alterations in shear stress is strongly associated with increased endothelial cell apoptosis *in vitro* (Pan et al., 2017) and *in vivo* (Heo et al., 2011), significant Bax expression at the adluminal surface was observed after flow restriction. Bcl-2/Bax ratios are an important rheostat to determine the incidence of apoptosis in general (Adams and Cory, 1998) and increases in Bax expression have been widely reported and validated using the TUNNEL assay to indicate apoptosis of endothelial cells *in vitro* in response to low shear stress (LSS) (Dong et al., 2017) and *in vivo* following carotid artery ligation in wildtype mice (Zhang et al., 2016) or following flow perturbation in ApoE deficient mice (Franck et al., 2017). The increase in Bax expression concomitant with an increase in the number of Sca1 cells that maintain a CD31 and eNOS endothelial cell phenotype at the adluminal surface is consistent with the appearance of new endothelial cells in the injured vessel that are derived from the proliferation of adluminal Sca1 cells. Indeed, recent cell fate mapping studies using Sca1-Cre-ERT2-tdT mice have since confirmed this observation by demonstrating that Sca1-CreERT marked cells expand in the intimal layer and maintain CDH5 endothelial cell fate following injury (Tang et al., 2020).

There are many potential reasons for the apparent differences in the outcomes of several lineage tracing studies that addressed the origin of lesional SMC-like cells including technical considerations around fixation, tissue preservation, brightness and contrast settings for image acquisition, autofluorescent material such as lipofuscin and single cell resolution (Bentzon and Majesky, 2018). Another important reason may involve the use of tamoxifen (Tm) in time-sensitive Tm-dependent Cre-LoxP models. Tm-induced Cre recombinase has been shown to indelibly mark cells up to 4 weeks after the last Tm injection thereby potentially confounding the interpretation of many previous studies (Reinert et al., 2012). In this context, we found that the fraction of S100β-CreER (tdT) marked cells within the various compartments of ligated vessels four weeks after the last Tm injection was similar to that observed after one week, indicating that, at least in our hands, medial SMC that might undergo de-differentiation and acquire the S100β promoter are not being inadvertently marked after injury.

Several GWAS studies have implicated HHIPL1 at the chromosome 14q32 CAD locus (van der Harst and Verweij, 2018; Schunkert et al., 2011) and identified it as a secreted Hh signaling protein that modulates atherosclerosis-relevant vascular phenotypes (Aravani et al., 2019). In the current study, we provide direct evidence that inhibition of Hh signalling controls neointimal thickening following flow restriction by attenuating the volume and accumulation of Sca1 cells within lesions. Furthermore Hh signalling directly promotes Sca1/S100β cells from mouse and S100β neuroectoderm stem cells derived from human induced pluripotent stem cells (HiPSC) to undergo myogenic differentiation to SMC-like cells *in vitro.* The former is not surprising as several previous studies support a role for Hh signalling in vascular lesion formation in mice (Beckers et al., 2007; Fitzpatrick et al., 2017; Redmond et al., 2013) where adventitial Sca1 stem cells co-localise with SHh and its receptor, Ptch1 (Passman et al., 2008). The possibility that Hh responsive S100β/Sca1 cells isolated from murine AA and TA regions are derived from a Myh11 medial SMC population was ruled out by examining the H3K4me2 epigenetic profile of S100β/Sca1 cells at the Myh11 locus, which is preserved during, at least some types of, SMC phenotypic modulation *in vitro* and *in vivo* following injury (Gomez et al., 2015; Shankman et al., 2015). Hh responsive S100β/Sca1 vSCs clearly do not have this SMC histone mark and only became enriched following myogenic differentiation to SMC-like cells, an effect attenuated by the Hh inhibitor, cylopamine. It appears the Yes-Associated Protein (YAP) is required for incorporation and expansion of Sca1-derived neointimal cells following injury (Tang et al., 2020) where the Hh pathway reportedly acts upstream of the Hippo pathway to regulate stem cell maintenance (Fernandez-L et al., 2009). Indeed, our data suggest S100β cells are also present in normal vessels within the adventitial layer where Hh components reside (Dunaeva et al., 2015; Queiroz et al., 2012). In arteriosclerotic lesions, S100β expression is exaggerated within the neointimal layer with sparse staining for PTCH1 present. As S100β NEP-derived SMCs are considered crucial to the generation of SMC in vascular lesions within atheroprone regions of the murine vasculature (Cheung et al., 2012; Sinha et al., 2014), it is tempting to speculate that Hh responsive S100β-derived SMC-like progeny may also play a pivotal role in lesion formation in humans. Future studies that address the interactions between Hippo pathway and Hh may yield therapeutic strategies aimed at interfering with YAP activity through inhibition of hedgehog pathway, which downregulates the YAP protein (Cotton et al., 2017; Felley-Bosco and Stahel, 2014)

In conclusion, the identification of a population of S100β/Sca1 cells within vascular lesions that are derived from a non-SMC S100β parent population is novel and an important source for intimal thickening following injury. Furthermore, the role of SHh in mediating this process expands our understanding of the mechanisms contributing to the progression of vascular lesions. While Hh signalling has previously been implicated in the development of vascular lesions through modulation of a differentiated SMC phenotype (Aravani et al., 2019), our study further suggests that Hh signalling may also control myogenic differentiation and accumulation S100β/Sca1 derived SMC-like progeny within vascular lesions. While hedgehog signalling appears critical, further research is required to investigate the precise mechanisms driving migration, proliferation and differentiation of stem cells during lesion formation. It is possible that SMC-like cells within lesions comprise several different stages of the myogenic, osteogenic and myeloid differentiation of various stem cells and hence display a variety of divergent phenotypes. The elucidation of these mechanisms will provide vital information needed for the development of more efficient and novel therapies for vascular proliferative diseases. Our results provide a potential strategy for the treatment of atherosclerosis by combating perivascular derived cell migration and asymmetric differentiation of a S100β parent vSC population.

Methods

Tamoxifen-induced genetic lineage tracing

S100β-CreER-Rosa26tdT mice (average weight 20g, 6-8 wks old) were injected IP with tamoxifen (Tm) dissolved in corn oil at 75 mg/kg for 5 consecutive days. Carotid artery ligation (partial, or complete), or sham operation, was performed at 1 wk or 4 wks after the last injection of Tm. At the indicated time post-ligation or sham operation, anesthetized mice were perfusion fixed and carotid arteries harvested for analysis.

Histomorphometry

At specified times post-ligation, mice were anesthetized (ketamine/xylazine) and perfusion fixed with 4% paraformaldehyde in sodium phosphate buffer (pH 7.0). Fixed carotids were embedded in paraffin for sectioning. Starting at the carotid bifurcation landmark (single lumen) a series of cross-sections (10 x 5 µm) were made, every 200 µm through 2 mm length of carotid artery. Cross-sections were de-paraffinized, rehydrated in graded alcohols and stained with Verhoeff-Van Gieson stain for elastic laminae and imaged using a Nikon TE300 microscope equipped with a Spot RT digital camera (Diagnostic Instruments). Digitized images were analyzed using SPOT Advanced imaging software. Assuming a circular structure in vivo, the circumference of the lumen was used to calculate the lumen area, the intimal area was defined by the luminal surface and internal elastic lamina (IEL), the medial area was defined by the IEL and external elastic lamina (EEL), and the adventitial area was the area between the EEL and the outer edge, essentially as described by us previously (Fitzpatrick et al., 2017)

Haematoxylin and Eosin Staining of Tissue

For human artery cross sections, slides were placed in ice-cold acetone and held at -20°C for 15 min. They were then washed 3 x PBS before immersion in Harris Haematoxylin at room temperature for 8 min. Slides were processed by sequential washing – in distilled water for 5 min; 1 % acid alcohol for 30 sec; 0.1 % sodium bicarbonate for 1 min and 95 % ethanol. Slides were then washed in Eosin for 1 min, 75 % ethanol for 3 min, 95 % ethanol for 3 min and 100 % ethanol for 3 min before being submerged in Histoclear for 3 min and permanently mounted using 3 drops of DPX, cleaned with 100 % ethanol before analysis.

For murine vessels, paraffin rehydration was conducted at room temperature by immersing the slides in xylene for 20 minutes. The slides were then immersed in the following gradients of ethanol for 5 minutes respectively: 100 %, 90 %, 70 % and 50 % ethanol. The slides were then rinsed in distilled H_2O_2 before washing in 1x PBS for 10 minutes. The slides were stored in 1x PBS until ready when they were immersed in Harris Haematoxylin at room temperature for 8 min.

Whole mount histochemical analysis

Briefly, arteries harvested from transgenic mice were washed in PBS before transfer to 10 % neutral buffered formalin and incubated at 4 °C overnight. The tissue was rinsed 3 x PBS before mounting on histology slides using DAPI containing fluoroshield. The whole tissue was then imaged using a Nikon Eclipse TS100 inverted microscope, EXFO X-Cite™ 120 fluorescence system and assessed using SPOT imaging software.

Immunofluorescent Staining of tissues.

Immunostaining essentially as previously described (Fitzpatrick et al., 2017). Carotid artery cryosections were air-dried for 1 h at room temperature, followed by incubation with blocking buffer (5% donkey serum, 0.1% Triton X-100 in PBS) for 30 minutes at room temperature and then incubated with primary antibody overnight at 4^0C in antibody solution (2.5% BSA, 0.3M Glycine and 1% Tween in DPBS). Murine and human arterial sections were stained with primary antibodies [Supplementary Table I]. Isotype IgG control and secondary antibody only controls were performed. For antigen retrieval, slides were brought to a boil in 10 mM sodium citrate (pH 6.0) then maintained at a sub-boiling temperature for 10 minutes. Slides were cooled on the bench-top for 30 minutes then washed in deionized water (3x5 min) each before being washed in PBS (3x5 min). The antigen retrieval protocol diminishes endogenous eGFP and Tdt tomato transgene signals. Therefore, those sections were co-stained with anti-eGFP antibody and anti-Td tomato antibody [Supplementary Table I].

For immunofluorescence staining, 5 consecutive images were obtained and processed using ImageJ software™ to analyze the collected images. Images were merged using the Image color-merge channels function. Merged signals and split channels were used to delineate the signals at single-cell resolution. Settings were fixed at the beginning of both acquisition and analysis steps and were unchanged. Brightness and contrast were lightly adjusted after merging.

Immunocytofluorescent staining of cells

Cells seeded onto UV sterilized coverslips were fixed with 3.7 % formaldehyde, (15 min, RT). If cells required permeabilization for the detection of intracellular antigens, cells were incubated in 0.025 % Triton X-100 PBS (room temp, 15 min). All coverslips were blocked (1 hr, RT) using 5 % BSA, 0.3 M Glycine, 1 % Tween PBS solution (1 hr, RT). Cells were incubated (how long?) with primary antibodies [Supplemental Table II], then washed twice with PBS to remove any unbound primary antibody before being incubated (1 hr, RT) with the recommended concentration of fluorochrome-conjugated secondary antibodies diluted in blocking buffer [Supplementary Table II]. Following 2x wash in PBS, cell nuclei were stained using DAPI: PBS (dilution 1:1000) (15 min, RT). For each primary and secondary antibody used, a secondary control and an IgG isotype control was performed to assess nonspecific binding. An Olympus CK30 microscope and FCell™ software was used to capture images. Images were analysed using ImageJ software as described above. Settings were fixed at the beginning of both acquisition and analysis steps and were unchanged. Brightness and contrast were lightly adjusted after merging.

Chromatin Immunoprecipitation

ChIP was performed on cultured cells as previously described with slight modifications (Gomez et al., 2013). Cells at 70% confluency were fixed with 1% paraformaldehyde (10 min, RT). Cross-link was stopped by addition of 125 mM glycine for 10 min. The cross-linked chromatin was sonicated to shear chromatin into fragments of 200–600 base pairs. The sheared chromatin was immunoprecipitated with 2 µg tri-methyl-histone H3 (Lys27) and di-methyl-histone H3 (Lys4), while negative control was incubated with mouse IgG and input DNA without antibody using the CHIP—IT Express HT Kit from Active Motif (Cat no: 53018) according to the manufacturer's instructions [Supplementary Table III]. A chromatin IP DNA Purification Kit (Cat No 58002 Active Motif) was used to purify the samples after CHIP before PCR was performed using Myh11 primers [5' -CCC TCC CTT TGC TAA ACA CA - 3' and 5' - CCA GAT CCT GGG TCC TTA CA – 3]. Sensimix SYBR® no-ROX Bioline Kit (QT650) was used to perform Real Time One-Step PCR according to the manufacturers' instructions. The antibodies used for ChIP are outlined in Supplemental Table I

Quantitative PCR

Total RNA was prepared from cultured cells using the ReliaPrep™ RNA Cell Miniprep System kit from Promega according to the manufacturer's protocol. Two micrograms of RNA was used for reverse transcription with Rotor-Gene SYBR Green RT-PCR (QIAGEN) or The SensiMix™ SYBR® No-ROX (BioLine) protocols for Real TimeOne-Step RT-PCR using the Real Time Rotor-GeneRG-3000™ light cycler from Corbett Research using primers listed in Supplementary Table IV.

Flow cytometry and analysis

Isolated cells were incubated with I fluorochrome-conjugated antibodies and control IgG's or (ii) the appropriate primary antibody with fluorochrome-conjugated secondary antibodies at a final concentration of 1µg per sample and incubated at 4°C for 30 minutes [Supplementary Table V]. Fluorescence labeled cells analysis was performed using a BD FACS Aria flow cytometry system (BD Biosciences), and data were analyzed with FlowJo™ software (Tree Star, Ashland, Ore) and De Novo software FCS Express 4 Flow Cytometry (Pasadena, CA)

Telomere Assay

The average telomere length in cells was measured using a ScienCell's Absolute Mouse Telomere Length Quantification qPCR Assay Kit (AMTLQ) according to the manufacturer's instructions. The telomere primer set recognizes and amplifies telomere sequences and is designed to directly measure the average telomere length of murine cells.

QUANTIFICATION AND STATISTICAL ANALYSIS

All data were determined from multiple individual biological samples and presented as mean values ± standard error of the mean (SEM). All in vitro experiments were performed in triplicate and repeated three times unless otherwise stated. All mice were randomly assigned to groups (including both male and female), and the analysis was performed blind by two groups. For statistical comparisons, all data was checked for normal gaussian distribution before parametric and non-parametric tests were performed. An unpaired two-sided Student's t-test was performed using GraphPad Prism software v8™ for comparing differences between two

groups, and ANOVA test for over multiple comparisons. Significance was accepted when $p \leq 0.05$.

EXPERIMENTAL MODEL AND SUBJECT DETAILS

Mice Breeding and Genotyping

All procedures were approved by the University of Rochester Animal Care Committee in accordance with the guidelines of the National Institutes of Health for the Care and Use of Laboratory Animals. Sca1-eGFP transgenic mice were obtained from JAX labs; Stock #012643, strain name B6.Cg.Tg(Ly6a-EGFP)G5Dzk/j. These transgenic mice have an enhanced green fluorescent protein (eGFP) under the control of murine lymphocyte antigen 6 complex, locus A (Ly6a) promoter. Hemizygous Ly6a-GFP mice are viable, fertile, normal in size and do not display any gross physical or behavioural abnormalities (Ma et al., 2002b).

S100β-EGFP/Cre/ERT2 transgenic mice (JAX Labs, stock #014160, strain name B6;DBA-Tg(S100β-EGFP/cre/ERT2)22Amc/j) express the eGFPCreER^{T2} (Enhanced Green Fluorescent Protein and tamoxifen inducible cre recombinase/ESR1) fusion gene under the direction of the mouse S100 promoter. Ai9 mice (Jax Labs, stock #007909, strain name B6.Cg-Gt(ROSA)26Sor$^{tm9(CAG\text{-}tdTomato)Hze}$ /J) express robust tdTomato fluorescence following Cre-mediated LoxP recombination. For lineage tracing experiments S100β-eGFP/Cre/ERT2–dTomato double transgenic mice of both genders were generated by crossing S100β-eGFP/Cre-ERT2 mice with Ai9 reporter mice. The tdTomato transgene expression pattern corresponds to genomically marked S100β, and the eGFP transgene expression pattern corresponds to current expression of S100β . Genomic DNA for genotyping was prepared from mice tail and papered for genotyping by Proteinase K lysed, isopropanol precipitated and 70% ethanol washed. The number of animals be used were approved based on the experimental effects size. All male and female mice were included in the study, and the start point (0 week) for each experiment involves adult mice of 8 weeks old.

Carotid Artery Ligation

Ligation of the left common carotid artery was performed essentially as described previously (Fitzpatrick et al., 2017) one and four weeks after Tm-induced cre-recombination, in male and female S100β-eGFP/Cre/ERT2–dTomato double transgenic mice. Prior to surgery mice received

a single dose of Buprenorphine SR (sustained release) analgesia (0.5-1.0 mg/kg SQ) (and every 72 hrs thereafter as needed). The animal was clipped and the surgical site prepped using betadine solution and alcohol. A midline cervical incision was made. For partial carotid artery ligation, with the aid of a dissecting microscope, the left external and internal carotid arterial branches were isolated and ligated with 6-0 silk suture reducing left carotid blood flow to flow via the patent occipital artery. The neck incision (2 layers, muscle and skin) was sutured closed. Partial ligation of the left carotid artery in this manner resulted in a decrease (~80%) in blood flow, leaving an intact endothelial monolayer. Buprenorphine was administered at least once post-op 6-12 hrs. For complete ligation, the left common carotid was isolated and ligated just beneath the bifurcation with 6-0 silk suture. In sham surgery group, carotid was similarly manipulated but not ligated. The neck incision (2 layers, muscle and skin) was sutured closed and the animal allowed recover under observation. After 3, 7, 14 and 21 days, mice were perfused with 4% PFA via the left ventricle for 10 min, and carotid arteries were harvested for analysis.

Cyclopamine treatment

Sca1-eGFP mice were treated with the smoothened inhibitor, cyclopamine, or the vehicle 2-hydropropyl-β-cyclodextrin (HβCD) (Sigma-Aldrich) alone as a control, (essentially as described by van den Brink (Van Den Brink et al., 2001). Mice were injected (250 µl max volume) intraperitoneally (IP) 1 day before ligation, then every other day after ligation at a dose of 10 mg/kg Cyclopamine (Sigma-Aldrich) dissolved in a solution of 45% (w/v) HβCD. There was no effect of cyclopamine treatment on mouse body weight, compared to the HβCD vehicle control group (data not shown).

Cell culture and harvesting

Murine aortic SMCs (MOVAS (ATCC® CRL-2797™) were cultured in Dulbeco's Modified Eagles growth medium (DMEM) supplemented with Fetal Bovine Serum (10%), L-glutamine (2 mM, Gibco) and Penicillin-Streptomycin (100U/mL, Gibco). Murine neuroectodermal stem cells (mNE-4Cs, ATCC® CRL-2925™) were grown in Eagle's Minimum Essential Medium supplemented with Fetal Bovine Serum (10%), L-glutamine (2 mM, Gibco) and Penicillin-Streptomycin (100U/mL, Gibco) using Poly-L-Lysine coated plates (15 µg/ml). Murine embryonic C3H 10T1/2 cells (ATCC® CRL-226™) were grown in Eagle's Basal medium

supplemented with heat-inactivated fetal bovine serum to a final concentration of 10% and 2mM L-glutamine. Murine embryonic stem cells (mESCs) ES-D3 [D3] (ATCC® CRL-1934™) were maintained in culture in Mouse ES Cell Basal Medium (ATCC SCRR-2011) supplemented with 2-mercaptoethanol (0.1 mM) and 15% ES-Cell Qualified FBS (ATCC SCRR-30-2020) and a 1,000 U/mL mouse leukemia inhibitory factor (LIF) (Millipore Cat. No. ESG1107). Murine vSCs from AA and TA regions of the mouse aorta were grown in DMEM media supplemented with chick embryo extract (2%), FBS embryonic qualified (1%, ATCC), B-27 Supplement, serum free, N-2 Supplement (Cell Therapy Systems), recombinant mouse bFGF (0.02 µg/mL), 2-Mercaptoethanol (50nM), retinoic acid (100 nM), Penicillin-Streptomycin (100U/mL, Gibco) (MM).

Isolation of S100β/Sca1 murine resident vascular stem cells (vSCs)

Using an optimised enzymatic cell dissociation technique protocol vSCs from both atheroprone (aortic arch - neuroectodermal, NE), and athero-resistant (thoracic aorta- paraxial mesodermal, PM) regions of the murine aorta were isolated using sequential seeding on adherent and non—adherent plates. Mouse thoracic aortas (4 at a time) were harvested and placed in cold Hank's solution for adipose tissue removal and lumen rinsing. The adventitia was enzymatically removed by incubation of the vessels in collagenase solution [i.e., MEM nucleosides GlutaMAX™ (2 ml) containing Collagenase type 1A (0.7 mg/ml), soybean trypsin inhibitor (50 mg/ml), and bovine serum albumin (1 mg/ml)] for approx. 10-20 min at 37°C. Once the adventitia became lose, it was carefully removed as an intact layer using forceps under a dissecting microscope. The aorta was divided into aortic arch (AA) and thoracic aorta (TA) regions and cut into 1 mm pieces and digested with Elastase type III (Sigma) at 37°C. Dispersed cells were centrifuged and washed twice in warm maintenance medium (MM) (DMEM supplemented with 2% chick embryo extract, 1% FBS, 0.02 µg/ml, bFGF basic protein, B-27 Supplement, N-2 supplement, 1% Penicillin-Streptomycin, 50 nM 2-Mercaptoethanol and 100 nM retinoic acid) before seeding (1st seeding) on a 6-well non-adherent plate in MM. At 48 h, suspension cells were transferred (2nd seeding) to a fresh well of a CELLstart™ pre-coated 6-well plate in MM. MM was added to the remaining cells in the non-adherent surface. Cells were incubated at 37°C, 5% CO_2 for 1 week with minimal disturbance. The stem cells exhibited a uniform neural-like morphology in low density culture adopting a dendritic-like tree shape and

retaining their morphological characteristics at low density throughout repeated passage. Cells were fed with MM every 2-3 days and passaged every 3-4 days or when ~70% confluent.

Generation of human neuroectoderm progenitors (NEPs) from induced pluripotent stem cells (HiPSCs)

Human induced pluripotent stem cells (HiPSC) were obtained from HipSci (Cambridge, UK) and cultured per the manufacturer's instructions. Briefly, human dermal fibroblasts were isolated from excess skin of patients undergoing plastic surgery and reprogrammed as previously described (Vallier et al., 2009). HiPSCs were grown on plates pre-coated using Vitronectin (10 µg/ml) and maintained in complete Essential eight medium replacing 95% of the medium daily. A ROCK inhibitor (10 µM) was added to optimize colony growth. Cells were sub-cultured with 0.05 mM EDTA for 4-8 min at room temperature until colonies displayed bright halos around the edges and small holes appeared throughout. Cells were frozen down in knock-out serum solution with 10% DMSO. HiPSCs at 70% confluency were routinely split at a ratio of 1:10 and cells were used between passage 20-40.

For neuroectoderm differentiation, cells were grown in chemically defined neuroectodermal medium (CDM) containing IMDM, F12 nutrient mix, chemically defined lipid concentrate, transferrin, monothioglycerol, penicillin-streptomycin and 0.5 g of PVA, and insulin, as previously described (Cheung et al., 2012). Neuroectoderm differentiation was initiated in CDM supplemented with FGF2 (12 ng/ml) and SB431542 (10 µM) for 7 days. Neuroectodermal (NE) progenitors were maintained in CDM-PVA supplemented with FGF2 (12 ng/ml) and SB431542 (10 µM) and sub-cultured using TrypLE™ for 3–5 min at 37°C in a 5% CO_2 incubator. NE progenitors were used between passage 1-10.

To initiate myogenic SMC differentiation, NEPs were subcultured in SMC differentiation medium containing CDM + PDGF-BB (10 ng/ml, PeproTech) + TGF-β1 (2 ng/ml, PeproTech) for 12 days. Neuroectoderm-derived SMCs (NE-SMC) were maintained in CDM supplemented with 10% FBS. After 12 d of PDGF-BB and TGF-β1 treatment, all cells appeared spindle-shaped. Complete medium was then changed to DMEM 10% FBS, 1% Penicillin streptomycin for expansion. Cells were frozen down using 90% (volume/volume) FBS + 10% (vol/vol) DMSO. The NE-SMC were used between passage 3-20.

Human tissue

Tissue sections from paired normal human aorta and arteriosclerotic vessels were obtained from Amsbio LLC, tissue repository.

Acknowledgments:

A. We thank Diana Scott for histological tissue processing, and Drs. Linda Callahan and Paivi Jordan for confocal microscope expertise.

B. This research was funded in part by Science Foundation Ireland grant SFI-11/PI/1128, Health Research Board (HRB) of Ireland grant HRA-POR-2015-1315, the European Union's INTERREG VA Programme, managed by the Special EU Programmes Body (SEUPB) to PAC, and NIH R21AA020365 and R21AA023213 to EMR, Irish Research Council (IRC) GOIPG/2014/43 (M.DiL) and GOIPG/2016/1529 (E.C), King Abdulla Scholarship IR15208 ID1066336148 to Y.G.

C. The authors declare no competing financial interests.

D. E.F., W.L., J-C.H, performed the animal experiments and M.DiL and SH performed the blind analysis of the images. E.F performed the human arteriosclerotic tissue analysis. E.F., M.DiL., R.H., D.B., E.C., performed the murine and rat cell culture experiments, D.B performed the HiPSCs cell work. EC performed the telomere assay and R.H.J, MdiL and Y.G., performed the ChIP analysis. E.M.R., C.L., and P.A.C drafted the manuscript, revised the manuscript and discussed the results. E.M.R., and P.A.C., designed and coordinated the experiments, interpreted the data, revised and confirmed the paper. All authors reviewed and confirmed the manuscript.

E. Correspondence to Paul A. Cahill (paul.cahill@dcu.ie) and Eileen M Redmond (Eileen_redmond@urmc.rochester.edu)

F. No datasets were generated or analysed during the current study.

Figure Legends

Figure 1. Expression of Sca1-eGFP and S100β-eGFP cells following iatrogenic flow restriction after 3 days.

A. Morphometric analysis of adventitial, medial, intimal and luminal volumes following partial ligation of the left carotid artery compared to sham controls. Data are the mean ± SEM of 4 animals, #p<0.05 vs sham.

B-D. The number of DAPI nuclei/hpf in cross-sections of (B) adventitia, (C) media and (D) intima following partial ligation of the left carotid artery (LCA) after 3d compared to untouched (control) and sham. Data are the mean ± SEM of 3-5 representative images per animals, n=3, #p<0.05.

E. Verhoeff-Van Gieson stained sections and corresponding confocal fluorescence images of DAPI nuclei (blue), Sca1-eGFP (green) and immunofluorescence of α-actin (SMA) (red), anti-eGFP (green), anti-CD31 (red) and anti-eNOS (red) expression in ligated LCA vessels expression in sham-operated and ligated LCA vessels. Arrows highlight Sca1-eGFP expressing cells in the adventitia (A), media (M) and neointima (NI) and CD31 and eNOS in intima. Scale bar = 20µm.

F. The fraction of Sca1 cells/high power field (hpf) in the adventitia, media, and intima of sham and ligated vessels after 3 days. Data are the mean ± SEM of 3- 5 sections, #p≤ 0.05 from a minimum of 4 animals per experimental group.

G. Representative immunofluorescence images for the pro-apoptotic marker, Bax, (red) in ligated left carotid artery (LCA) vessels and contralateral right carotid artery (RCA) after 3d. IgG was used as a control.

H. The number of Bax cells/hpf in the adventitia, media, and intima of sham and ligated vessels after 3d. Arrows highlight Bax expressing cells within the adventitia (A), media (M), and neointima (NI). Data are the mean ± SEM of 3-6 sections per experimental group from 3 animals. #p≤ 0.05. Scale bar = 20µm.

Figure 2. **Expression of Sca1-eGFP and S100β-eGFP cells following iatrogenic flow restriction after 7, 14 and 21 days.**

A-B. Representative Verhoeff-Van Gieson stained sections and corresponding confocal fluorescence images of DAPI nuclei (blue) and Sca1-eGFP (green) expression in LCA after (A) 7 days and (B) 14 days. Scale bar = 20µm.

C-D. The number of DAPI nuclei/hpf in cross-sections of adventitia, media and intima following partial ligation of the LCA after 7d and 14d compared to sham. Data are the mean ± SEM of 3-5 representative images per animals, n=3, #p<0.05.

E-F. The fraction of Sca1 cells/ high power field (hpf) in the adventitia, media, and intima of sham and ligated vessels after (E) 7 days and (F) 14 days. Data are the mean ± SEM of 10-15 sections, #p≤0.05 from a minimum of 4 animals per experimental group.

G. Representative confocal fluorescence images of DAPI nuclei (blue) and S100β-eGFP (green) expression in the contralateral RCA and LCA from sham and ligated vessels. Scale bar = 20µm.

H. Representative confocal fluorescence images of DAPI nuclei (blue), immunofluorescence of anti-eGFP (green) expression and anti-Sca1 (far red, white) in the RCA and LCA 21 days post-ligation in S100β-eGFP mice. Data are from a minimum of 3 animals per experimental group. Scale bar = 20µm.

I. Representative confocal fluorescence images of DAPI nuclei (blue), immunofluorescence of anti-eGFP (green) expression and anti-SMA (Red) in the LCA 14 days post-ligation in Sca1-eGFP mice. Data are representative of 5 images per animal.

J. Representative confocal fluorescence images of DAPI nuclei (blue), immunofluorescence of anti-eGFP (green) expression and anti-Sca1 (far red, white) in the LCA 21 days post-ligation in S100β-eGFP mice.

K-L. Cumulative analysis of the fraction of S100β-eGFP cells in the adventitia (A), media (M), and neointima (NI) of (K) contralateral RCA and (L) LCA 21 days post-ligation in S100β-eGFP mice. Data are the mean ± SEM, n=15-20 sections from 5 animals, #p≤ 0.05 vs Sham.

M. Cumulative analysis of the fraction of double positive S100β/Sca1 cells within the adventitia (A), media (M), and neointima (NI) of contralateral RCA and ligated LCA 21 days post-ligation in S100β-eGFP mice. Data are the mean ± SEM of five sections from 3 animals #p≤ 0.05 vs Sham.

Figure 3. Lineage tracing analysis of S100β-Cre(ERT2)-tdT marked cells following iatrogenic flow restriction for 21 days.

A-C. (A) Verhoeff-Van Gieson stained sections and morphometric analysis of adventitial, medial, intimal and luminal volumes of the (B) contralateral RCA control compared to the (C) LCA following ligation for 21d. Data are the mean ± SEM of 10 images, #p<0.05 vs sham controls.

D-F. Representative confocal fluorescence images of DAPI nuclei (blue) and S100β-tdT (red) cells in mice treated with corn oil (control) or tamoxifen for 7 days prior to washout for 1 week in (D) sham and (E-F) ligated LCA. Data are minimum of 4 animals per experimental group. Scale bar = 20 µm. Arrows highlight S100β-tdT (red) expressing cells within the adventitia (A), media (M), and neointima (NI).

G. Representative confocal fluorescence images of DAPI nuclei (blue), immunofluorescence of anti-tdT (red) and anti-Sca1 (far red, white) expression in the contralateral RCA and LCA 21 days post ligation. Scale bar = 20µm.

H. Cumulative analysis of the fraction of S100β-tdT$^+$ cells within the adventitia (A), media (M), and neointima (NI) of sham and ligated LCA. Data are the mean ± SEM of 15-20 sections per experimental group, #p≤ 0.05 from 4 animals per group. **I-J.** Cumulative analysis of the (I) fraction of S100β/Sca1 cells and (J) percent of S100β-tdT$^+$ cells that are Sca1 within the adventitia (A), media (M), and neointima (NI) of contralateral RCA and ligated LCA. Data are the mean ± SEM 10-15 sections from 3 animals per group, #p≤ 0.05 vs Sham

Figure 4. Inhibition of Hh signalling attenuates intimal thickening and Sca1 cell expansion following iatrogenic flow restriction.

A. Representative immunofluorescence images of Hh receptor patched 1 (Ptch1) (red), Hh target gene Gli2 (red), Sca1-eGFP (green) expression and merged (eGFP/Gli2/DAPI) in carotid

artery cross sections from sham-operated, ligated vehicle control (HβCD), and ligated + cyclopamine (10 mg/kg, IP) treated mice after 14 days. Scale bar = top panel: 50µm, all other panels: 20µm.

B-C. Cumulative data showing the fraction of Sca1-eGFP cells within the adventitia (A), media (M), and neointima (NI) from sham-operated, ligated vehicle control (HβCD), and ligated + cyclopamine (Cyl) Sca1-eGFP mice after (B) 7 days and (C) 14 days. Data are the mean ± SEM of five sections per experimental group, #p≤ 0.05 vs ligated HβCD controls and are representative of a minimum of 4 animals per experimental group.

D-E. Representative H&E staining of carotid artery cross sections from sham, ligated control (HβCD vehicle), and ligated + cyclopamine (Cyl) treated animals after 7 d (D) and 14 d (E). Scale bar = 50 µm.

F-G. Vessel compartment volumes for ligated control (HβCD), and ligated + cyclopamine (Cyl) treated animals after (F) 7d and (G) 14 d. Data mean ± SEM of 7-12 sections analysed from 4 animals, #p≤ 0.05 vs ligated control (HβCD).

Figure 5. Resident S100β/Sca1 vascular stem cells from atheroprone and atheroresistant regions of the mouse aorta *in vitro.*

A. Relative levels of *Myh11* and *Cnn1* in AA and TA regions of the mouse aorta. Data are expressed as the Log2 fold change in mRNA levels relative to neural stem cells (NE-4C) in culture and are the mean ± SEM of three aortic specimens, #p≤ 0.05 vs NE-4C cells. The housekeeping gene *Gapdh* was used as a control.

B-C. The level of enrichment of mRNA for neuroectodermal markers (B) S100β and (C) Sox10 within atheroprone AA (aortic arch) and atheroresistant TA (thoracic/descending aorta) regions of the mouse aorta in the absence or presence of the adventitial (Adv) layer. The housekeeping gene *hypoxanthine guanine phosphoribosyltransferase* (*hprt*) was used as a control. Data are expressed as the Log2 fold change in mRNA levels relative to murine aortic SMCs in culture and are the mean ± SEM of three aortic specimens, #p≤ 0.05 vs MOVAS SMCs.

D. Representative immunocytochemical analysis of stem cell markers S100β, Nestin, Sox10, Sox17, Sca1 and SMC differentiation markers, Cnn1 and Myh11 in vSCs isolated and grown in maintenance media (MM) from AA and TA regions of the mouse aorta. Scale bar 20µm.

E. Flow cytometry analysis of vSCs isolated from AA and TA regions of the mouse aorta and grown in maintenance media for S100β (dark green) and Sca1 (light green) expression. NE-4C and CH3-10T1/2 cells were used as positive controls, respectively. Filled dark and light green curves represent negative control samples.

F-G. Relative levels of (F) *Myh11* and (G) *Cnn1* in vSCs isolated from AA and TA regions of the mouse aorta, compared to AA and TA aortic tissue. Data are expressed as the Log2 fold change in mRNA levels relative to neural stem cells (NE-4C) in culture and are the mean ± SEM of three independent cultures and three aortic specimens, #p≤ 0.05 vs NE-4C cells.

H. Absolute telomere length of vSCs compared to cultured MOVAS SMC and fresh aortic tissue. The telomere primer set recognizes and amplifies telomere sequences. The single copy reference (SCR) primer set recognizes and amplifies a 100 bp-long region on mouse chromosome 10, and serves as reference for data normalization. Data are expressed as absolute telomere length (kb) and are the mean ± SEM of three plates and aortic specimens, #p≤ 0.05 vs MOVAs SMCs.

I-J. Relative levels of *Gli1*, *Myh11* and *Cnn1* within vSCs isolated from (I) AA and (J) TA regions of the mouse aorta in the absence or presence of rSHh (0.5 µg/ml) with or without the smoothened inhibitor, cyclopamine (10µM). Data are expressed as the Log2 fold change in mRNA levels relative to vSCs alone (control) and are the mean ± SEM of three representative wells from two independent experiments, #p≤0.05 versus rSHh alone.

K. ChiP analysis of the level of enrichment of (K) H3K4me2 at the *Myh11* locus in AA vSCs in the absence or presence of rSHh (0.5 µg/ml) with or without cyclopamine (15µM) for 7 d. Fresh aortic tissue and mouse ECSs was used as positive and negative controls, respectively.

M-N. The ratio of (M) H3K4me2:H3K27me3 and (N) H3K27me3:H3K4me2 enrichment at the *Myh11* locus in AA vSCs in the absence or presence of rSHh (0.5 µg/ml) with or without cyclopamine (10µM) for 7 d. Data are the mean ± SEM, n=3, #p≤ 0.05 versus aorta/ESC, *p≤ 0.05 vs vSC, §p≤ 0.05 vs rSHh

N-O. Representative immunocytofluorescence staining and the fraction of Cnn1 and Myh11 positive cells in the absence or presence of rSHh (0.5 µg/ml) with or without cyclopamine (15µM) for 7 days. Representative images shown, Scale bar = 50 µm. Cumulative data is the mean ± SEM, n=3, #p≤ 0.05 versus control, *p≤ 0.05 vs rSHh.

Figure 6. Human neuroectoderm progenitors express S100β cells and are present in vascular lesions.

A. Representative phase contrast photomicrographs, hematoxylin and eosin (H&E) staining, DAPI staining (blue) and immunocytochemical staining for smooth muscle cell α-actin (SMA) (red), S100β (red) and PTCH1 as indicated in the adventitial (A), medial (M), and intimal (I) sections of human normal and arteriosclerotic arteries. Scale bar=50µm. Data are representative of 3 sections from 3 patient cohorts.

B. Phase contrast images, fluorescence staining of DAPI nuclei (blue) and immunoctytochemical analysis of the expression of OCT4 (green), S100β (green) in NEPs and CNN1 (green) and MYH11 (green) in NEP-derived SMCs. All cells were generated as described previously (Cheung et al., 2012). Scale bar = Right panels: 50µm, Left panels: 20µm. Data are representative of five images per experimental group from three independent cultures.

C. The fraction of B S100β, C $CNN1^+$ and D $MYH11^+$ cells in HiPSCs, NEPs and NEP-SMCs. Data are mean ± SEM, n=3, #p≤ 0.05 versus HiPSCs.

D-F. Relative levels of S100β, CNN1 and MYH11 in HiPSCs, NEPs and NEP-SMCs, respectively. Data are expressed as the Log2 fold change in mRNA levels relative to HiPSCs in culture and are the mean ± SEM, n=3, #p≤ 0.05 versus HiPSCs.

G-H. Relative levels of CNN1 and MYH11 in NEPs in the absence or presence of hSHh (0.5µg/ml) with or without cyclopamine (15µM) for 12 d. Data are representative of three independent cultures, #p≤ 0.05 versus NEPs, *p≤ 0.05 vs hSHh.

H. Immunoctytochemical analysis of CNN1 (green) expression and DAPI (blue) staining in NEPs in the absence or presence of recombinant hSHh (1.0 µg/ml) for 12 d. Data are representative of five images per experimental group from two independent cultures.

Bibliography

Adams, J.M., and Cory, S. (1998). The Bcl-2 protein family: Arbiters of cell survival. Science (80-.). *281*, 1322–1326.

Ali, H., Emoto, N., Yagi, K., Vignon-Zellweger, N., Nakayama, K., Hatakeyama, K., Asada, Y., Rikitake, Y., and Hirata, K.-I. (2013). Localization and characterization of a novel secreted protein, SCUBE2, in the development and progression of atherosclerosis. Kobe J. Med. Sci. *59*, E122-31.

Aravani, D., Morris, G.E., Jones, P.D., Tattersall, H.K., Karamanavi, E., Kaiser, M.A., Kostogrys, R.B., Ghaderi Najafabadi, M., Andrews, S.L., Nath, M., et al. (2019). *HHIPL1* , a Gene at the 14q32 Coronary Artery Disease Locus, Positively Regulates Hedgehog Signaling and Promotes Atherosclerosis. Circulation *140*, 500–513.

Baker, A.H., and Péault, B. (2016). A Gli(1)ttering Role for Perivascular Stem Cells in Blood Vessel Remodeling. Cell Stem Cell *19*, 563–565.

Basatemur, G.L., Jørgensen, H.F., Clarke, M.C.H., Bennett, M.R., and Mallat, Z. (2019). Vascular smooth muscle cells in atherosclerosis. Nat. Rev. Cardiol. *16*, 727–744.

Beckers, L., Heeneman, S., Wang, L., Burkly, L.C., Rousch, M.M.J., Davidson, N.O., Gijbels, M.J.J., de Winther, M.P.J., Daemen, M.J.A.P., and Lutgens, E. (2007). Disruption of hedgehog signalling in ApoE - /- mice reduces plasma lipid levels, but increases atherosclerosis due to enhanced lipid uptake by macrophages. J. Pathol. *212*, 420–428.

Bennett, M.R., Sinha, S., and Owens, G.K. (2016). Vascular Smooth Muscle Cells in Atherosclerosis. Circ. Res. *118*, 692–702.

Bentzon, J.F., and Majesky, M.W. (2018). Lineage tracking of origin and fate of smooth muscle cells in atherosclerosis. Cardiovasc. Res. *114*, 492–500.

Van Den Brink, G.R., Hardwick, J.C.H., Peppelenbosch, M.P., Van Deventer, S.J.H., Tytgat, G.N.J., Brink, M.A., and Ten Kate, F.J. (2001). Sonic hedgehog regulates gastric gland morphogenesis in man and mouse. Gastroenterology *121*, 317–328.

Briscoe, J., and Thérond, P.P. (2013). The mechanisms of Hedgehog signalling and its roles in

development and disease. Nat. Rev. Mol. Cell Biol. *14*, 416–429.

Campbell, G.J., and Roach, M.R. Fenestrations in the internal elastic lamina at bifurcations of human cerebral arteries. Stroke *12*, 489–496.

Campbell, J.H., and Campbell, G.R. (2012). Smooth Muscle Phenotypic Modulation—A Personal Experience. Arterioscler. Thromb. Vasc. Biol. *32*, 1784–1789.

Cao, T., Zhang, L., Yao, L.-L., Zheng, F., Wang, L., Yang, J.-Y., Guo, L.-Y., Li, X.-Y., Yan, Y.-W., Pan, Y.-M., et al. (2017). S100B promotes injury-induced vascular remodeling through modulating smooth muscle phenotype. Biochim. Biophys. Acta. Mol. Basis Dis. *1863*, 2772–2782.

Chakraborty, R., Saddouk, F.Z., Carrao, A.C., Krause, D.S., Greif, D.M., and Martin, K.A. (2019). Promoters to Study Vascular Smooth Muscle. Arterioscler. Thromb. Vasc. Biol. *39*, 603–612.

Chappell, J., Harman, J.L., Narasimhan, V.M., Yu, H., Foote, K., Simons, B.D., Bennett, M.R., and Jørgensen, H.F. (2016). Extensive Proliferation of a Subset of Differentiated, yet Plastic, Medial Vascular Smooth Muscle Cells Contributes to Neointimal Formation in Mouse Injury and Atherosclerosis Models. Circ. Res. *119*, 1313–1323.

Chen, Q., Yang, M., Wu, H., Zhou, J., Wang, W., Zhang, H., Zhao, L., Zhu, J., Zhou, B., Xu, Q., et al. (2018). Genetic lineage tracing analysis of c-kit+ stem/progenitor cells revealed a contribution to vascular injury-induced neointimal lesions. J. Mol. Cell. Cardiol. *121*, 277–286.

Cheung, C., Bernardo, A.S., Trotter, M.W.B., Pedersen, R.A., and Sinha, S. (2012). Generation of human vascular smooth muscle subtypes provides insight into embryological origin-dependent disease susceptibility. Nat. Biotechnol. *30*, 165–173.

Chuang, P.T., and McMahon, A.P. (1999). Vertebrate hedgehog signalling modulated by induction of a hedgehog- binding protein. Nature *397*, 617–621.

Cooley, B.C., Nevado, J., Mellad, J., Yang, D., St. Hilaire, C., Negro, A., Fang, F., Chen, G., San, H., Walts, A.D., et al. (2014). TGF- Signaling Mediates Endothelial-to-Mesenchymal Transition (EndMT) During Vein Graft Remodeling. Sci. Transl. Med. *6*, 227ra34-227ra34.

Cotton, J.L., Li, Q., Ma, L., Park, J.-S., Wang, J., Ou, J., Zhu, L.J., Ip, Y.T., Johnson, R.L., and Mao, J. (2017). YAP/TAZ and Hedgehog Coordinate Growth and Patterning in Gastrointestinal

Mesenchyme. Dev. Cell *43*, 35-47.e4.

Dobnikar, L., Taylor, A.L., Chappell, J., Oldach, P., Harman, J.L., Oerton, E., Dzierzak, E., Bennett, M.R., Spivakov, M., and Jørgensen, H.F. (2018). Disease-relevant transcriptional signatures identified in individual smooth muscle cells from healthy mouse vessels. Nat. Commun. *9*, 4567.

Donato, R., Sorci, G., Riuzzi, F., Arcuri, C., Bianchi, R., Brozzi, F., Tubaro, C., and Giambanco, I. (2009). S100B's double life: intracellular regulator and extracellular signal. Biochim. Biophys. Acta *1793*, 1008–1022.

Dong, G., Yang, S., Cao, X., Yu, N., Yu, J., and Qu, X. (2017). Low shear stress-induced autophagy alleviates cell apoptosis in HUVECs. Mol. Med. Rep. *15*, 3076–3082.

Dunaeva, M., van Oosterhoud, C., and Waltenberger, J. (2015). Expression of Hedgehog signaling molecules in human atherosclerotic lesions: An autopsy study. Int. J. Cardiol. *201*, 462–464.

Dutzmann, J., Koch, A., Weisheit, S., Sonnenschein, K., Korte, L., Haertlé, M., Thum, T., Bauersachs, J., Sedding, D.G., and Daniel, J.-M. (2017). Sonic hedgehog-dependent activation of adventitial fibroblasts promotes neointima formation. Cardiovasc. Res. *113*, 1653–1663.

Felley-Bosco, E., and Stahel, R. (2014). Hippo/YAP pathway for targeted therapy. Transl. Lung Cancer Res. *3*, 75–83.

Fernandez-L, A., Northcott, P.A., Dalton, J., Fraga, C., Ellison, D., Angers, S., Taylor, M.D., and Kenney, A.M. (2009). YAP1 is amplified and up-regulated in hedgehog-associated medulloblastomas and mediates Sonic hedgehog-driven neural precursor proliferation. Genes Dev. *23*, 2729–2741.

Fitzpatrick, E., Han, X., Liu, W., Corcoran, E., Burtenshaw, D., Morrow, D., Helt, J.-C., Cahill, P.A., and Redmond, E.M. (2017). Alcohol Reduces Arterial Remodeling by Inhibiting Sonic Hedgehog-Stimulated Stem Cell Antigen-1 Positive Progenitor Stem Cell Expansion. Alcohol. Clin. Exp. Res. *41*, 2051–2065.

Franck, G., Mawson, T., Sausen, G., Salinas, M., Masson, G.S., Cole, A., Beltrami-Moreira, M., Chatzizisis, Y., Quillard, T., Tesmenitsky, Y., et al. (2017). Flow Perturbation Mediates

Neutrophil Recruitment and Potentiates Endothelial Injury via TLR2 in Mice: Implications for Superficial Erosion. Circ. Res. *121*, 31–42.

Gomez, D., and Owens, G.K. (2016). Reconciling Smooth Muscle Cell Oligoclonality and Proliferative Capacity in Experimental Atherosclerosis. Circ. Res. *119*, 1262–1264.

Gomez, D., Shankman, L.S., Nguyen, A.T., and Owens, G.K. (2013). Detection of histone modifications at specific gene loci in single cells in histological sections. Nat. Methods *10*, 171–177.

Gomez, D., Swiatlowska, P., and Owens, G.K. (2015). Epigenetic Control of Smooth Muscle Cell Identity and Lineage Memory. Arterioscler. Thromb. Vasc. Biol. *35*, 2508–2516.

Guo, Z.-Y., Yan, Z.-Q., Bai, L., Zhang, M.-L., and Jiang, Z.-L. (2008). Flow shear stress affects macromolecular accumulation through modulation of internal elastic lamina fenestrae. Clin. Biomech. *23*, S104–S111.

Halcox, J.P.J., Donald, A.E., Ellins, E., Witte, D.R., Shipley, M.J., Brunner, E.J., Marmot, M.G., and Deanfield, J.E. (2009). Endothelial Function Predicts Progression of Carotid Intima-Media Thickness. Circulation *119*, 1005–1012.

van der Harst, P., and Verweij, N. (2018). Identification of 64 Novel Genetic Loci Provides an Expanded View on the Genetic Architecture of Coronary Artery Disease. Circ. Res. *122*, 433–443.

Hayashi, A., Koob, J.W., Liu, D.Z., Tong, A.Y., Hunter, D.A., Parsadanian, A., Mackinnon, S.E., and Myckatyn, T.M. (2007). A double-transgenic mouse used to track migrating Schwann cells and regenerating axons following engraftment of injured nerves. Exp. Neurol. *207*, 128–138.

Heo, K.-S., Lee, H., Nigro, P., Thomas, T., Le, N.-T., Chang, E., McClain, C., Reinhart-King, C.A., King, M.R., Berk, B.C., et al. (2011). PKCζ mediates disturbed flow-induced endothelial apoptosis via p53 SUMOylation. J. Cell Biol. *193*, 867–884.

Herring, B., Hoggatt, A.M., Burlak, C., and Offermanns, S. (2014). Previously differentiated medial vascular smooth muscle cells contribute to neointima formation following vascular injury. Vasc. Cell *6*, 21.

Hoglund, V.J., Dong, X.R., and Majesky, M.W. (2010). Neointima formation: a local affair. Arterioscler. Thromb. Vasc. Biol. *30*, 1877–1879.

Hromada, C., Mühleder, S., Grillari, J., Redl, H., and Holnthoner, W. (2017). Endothelial Extracellular Vesicles-Promises and Challenges. Front. Physiol. *8*, 275.

Hu, Y., Zhang, Z., Torsney, E., Afzal, A.R., Davison, F., Metzler, B., and Xu, Q. (2004). Abundant progenitor cells in the adventitia contribute to atherosclerosis of vein grafts in ApoE-deficient mice. J. Clin. Invest. *113*, 1258–1265.

Ingham, P.W., and McMahon, A.P. (2001). Hedgehog signaling in animal development: Paradigms and principles. Genes Dev. *15*, 3059–3087.

Kennedy, E., Hakimjavadi, R., Greene, C., Mooney, C.J., Fitzpatrick, E., Collins, L.E., Loscher, C.E., Guha, S., Morrow, D., Redmond, E.M., et al. (2014). Embryonic rat vascular smooth muscle cells revisited - a model for neonatal, neointimal SMC or differentiated vascular stem cells? Vasc. Cell *6*, 6.

Korshunov, V.A., and Berk, B.C. (2003). Flow-induced vascular remodeling in the mouse: a model for carotid intima-media thickening. Arterioscler. Thromb. Vasc. Biol. *23*, 2185–2191.

Kramann, R., Goettsch, C., Wongboonsin, J., Iwata, H., Schneider, R.K., Kuppe, C., Kaesler, N., Chang-Panesso, M., Machado, F.G., Gratwohl, S., et al. (2016). Adventitial MSC-like Cells Are Progenitors of Vascular Smooth Muscle Cells and Drive Vascular Calcification in Chronic Kidney Disease. Cell Stem Cell *19*, 628–642.

Li, F., Duman-Scheel, M., Yang, D., Du, W., Zhang, J., Zhao, C., Qin, L., and Xin, S. (2010). Sonic hedgehog signaling induces vascular smooth muscle cell proliferation via induction of the G1 cyclin-retinoblastoma axis. Arterioscler. Thromb. Vasc. Biol. *30*, 1787–1794.

Liu, W., Redmond, E.M., Morrow, D., and Cullen, J.P. (2011). Differential effects of daily-moderate versus weekend-binge alcohol consumption on atherosclerotic plaque development in mice. Atherosclerosis *219*, 448–454.

López-Mejías, R., Corrales, A., Vicente, E., Robustillo-Villarino, M., González-Juanatey, C., Llorca, J., Genre, F., Remuzgo-Martínez, S., Dierssen-Sotos, T., Miranda-Filloy, J.A., et al. (2017). Influence of coronary artery disease and subclinical atherosclerosis related

polymorphisms on the risk of atherosclerosis in rheumatoid arthritis. Sci. Rep. *7*, 40303.

Ma, X., Robin, C., Ottersbach, K., and Dzierzak, E. (2002a). The *Ly‐6A* (Sca‐1) *GFP* Transgene is Expressed in all Adult Mouse Hematopoietic Stem Cells. Stem Cells *20*, 514–521.

Ma, X., Robin, C., Ottersbach, K., and Dzierzak, E. (2002b). The *Ly‐6A* (Sca‐1) *GFP* Transgene is Expressed in all Adult Mouse Hematopoietic Stem Cells. Stem Cells *20*, 514–521.

Majesky, M.W., Horita, H., Ostriker, A., Lu, S., Regan, J.N., Bagchi, A., Dong, X.R., Poczobutt, J., Nemenoff, R.A., and Weiser-Evans, M.C.M. (2017). Differentiated Smooth Muscle Cells Generate a Subpopulation of Resident Vascular Progenitor Cells in the Adventitia Regulated by Klf4. Circ. Res. *120*, 296–311.

Marigo, V., and Tabin, C.J. (1996). Regulation of patched by Sonic hedgehog in the developing neural tube. Proc. Natl. Acad. Sci. U. S. A. *93*, 9346–9351.

Marigo, V., Davey, R.A., Zuo, Y., Cunningham, J.M., and Tabin, C.J. (1996a). Biochemical evidence that patched is the hedgehog receptor. Nature *384*, 176–179.

Marigo, V., Johnson, R.L., Vortkamp, A., and Tabin, C.J. (1996b). Sonic hedgehog differentially regulates expression of GLI and GLI3 during limb development. Dev. Biol. *180*, 273–283.

Moonen, J.-R.A.J., Lee, E.S., Schmidt, M., Maleszewska, M., Koerts, J.A., Brouwer, L.A., van Kooten, T.G., van Luyn, M.J.A., Zeebregts, C.J., Krenning, G., et al. (2015). Endothelial-to-mesenchymal transition contributes to fibro-proliferative vascular disease and is modulated by fluid shear stress. Cardiovasc. Res. *108*, 377–386.

Morrow, D., Cullen, J.P., Liu, W., Guha, S., Sweeney, C., Birney, Y.A., Collins, N., Walls, D., Redmond, E.M., and Cahill, P.A. (2009). Sonic Hedgehog induces Notch target gene expression in vascular smooth muscle cells via VEGF-A. Arterioscler. Thromb. Vasc. Biol. *29*, 1112–1118.

Murgai, M., Ju, W., Eason, M., Kline, J., Beury, D.W., Kaczanowska, S., Miettinen, M.M., Kruhlak, M., Lei, H., Shern, J.F., et al. (2017). KLF4-dependent perivascular cell plasticity mediates pre-metastatic niche formation and metastasis. Nat. Med. *23*, 1176–1190.

Murry, C.E., Gipaya, C.T., Bartosek, T., Benditt, E.P., and Schwartz, S.M. (1997). Monoclonality of smooth muscle cells in human atherosclerosis. Am. J. Pathol. *151*, 697–705.

Nam, D., Ni, C.-W., Rezvan, A., Suo, J., Budzyn, K., Llanos, A., Harrison, D., Giddens, D., and Jo, H. (2009). Partial carotid ligation is a model of acutely induced disturbed flow, leading to rapid endothelial dysfunction and atherosclerosis. Am. J. Physiol. Heart Circ. Physiol. *297*, H1535-43.

Nemenoff, R.A., Horita, H., Ostriker, A.C., Furgeson, S.B., Simpson, P.A., VanPutten, V., Crossno, J., Offermanns, S., and Weiser-Evans, M.C.M. (2011). SDF-1α induction in mature smooth muscle cells by inactivation of PTEN is a critical mediator of exacerbated injury-induced neointima formation. Arterioscler. Thromb. Vasc. Biol. *31*, 1300–1308.

Nguyen, A.T., Gomez, D., Bell, R.D., Campbell, J.H., Clowes, A.W., Gabbiani, G., Giachelli, C.M., Parmacek, M.S., Raines, E.W., Rusch, N.J., et al. (2013). Smooth muscle cell plasticity: fact or fiction? Circ. Res. *112*, 17–22.

Owens, G.K. (2007). Molecular control of vascular smooth muscle cell differentiation and phenotypic plasticity. Novartis Found. Symp. *283*, 174–191; discussion 191-3, 238–241.

Pan, L., Hong, Z., Yu, L., Gao, Y., Zhang, R., Feng, H., Su, L., and Wang, G. (2017). Shear stress induces human aortic endothelial cell apoptosis via interleukin-1 receptor-associated kinase 2-induced endoplasmic reticulum stress. Mol. Med. Rep. *16*, 7205–7212.

Passman, J.N., Dong, X.R., Wu, S.-P., Maguire, C.T., Hogan, K.A., Bautch, V.L., and Majesky, M.W. (2008). A sonic hedgehog signaling domain in the arterial adventitia supports resident Sca1+ smooth muscle progenitor cells. Proc. Natl. Acad. Sci. U. S. A. *105*, 9349–9354.

Pawlowski, J., and Kraft, A.S. (2000). Bax-induced apoptotic cell death. Proc. Natl. Acad. Sci. U. S. A. *97*, 529–531.

Petrova, R., and Joyner, A.L. (2014). Roles for Hedgehog signaling in adult organ homeostasis and repair. Dev. *141*, 3445–3457.

Psaltis, P.J., Puranik, A.S., Spoon, D.B., Chue, C.D., Hoffman, S.J., Witt, T.A., Delacroix, S., Kleppe, L.S., Mueske, C.S., Pan, S., et al. (2014). Characterization of a resident population of adventitial macrophage progenitor cells in postnatal vasculature. Circ. Res. *115*, 364–375.

Queiroz, K.C.S., Bijlsma, M.F., Tio, R.A., Zeebregts, C.J., Dunaeva, M., Ferreira, C. V, Fuhler, G.M., Kuipers, E.J., Alves, M.M., Rezaee, F., et al. (2012). Dichotomy in Hedgehog signaling between human healthy vessel and atherosclerotic plaques. Mol. Med. *18*, 1122–1127.

Redmond, E.M., Hamm, K., Cullen, J.P., Hatch, E., Cahill, P.A., and Morrow, D. (2013). Inhibition of patched-1 prevents injury-induced neointimal hyperplasia. Arterioscler. Thromb. Vasc. Biol. *33*, 1960–1964.

Reinert, R.B., Kantz, J., Misfeldt, A.A., Poffenberger, G., Gannon, M., Brissova, M., and Powers, A.C. (2012). Tamoxifen-Induced Cre-loxP Recombination Is Prolonged in Pancreatic Islets of Adult Mice. PLoS One *7*, e33529.

Roostalu, U., Aldeiri, B., Albertini, A., Humphreys, N., Simonsen-Jackson, M., Wong, J.K.F., and Cossu, G. (2018). Distinct Cellular Mechanisms Underlie Smooth Muscle Turnover in Vascular Development and Repair. Circ. Res. *122*, 267–281.

Sagheddu, R., Chiappalupi, S., Salvadori, L., Riuzzi, F., Donato, R., and Sorci, G. (2018). Targeting RAGE as a potential therapeutic approach to Duchenne muscular dystrophy. Hum. Mol. Genet. *27*, 3734–3746.

Sakamoto, A., Torii, S., Jinnouchi, H., Finn, A. V, Virmani, R., and Kolodgie, F.D. (2018). Pathologic intimal thickening: Are we any closer to understand early transitional plaques that lead to symptomatic disease? Atherosclerosis *274*, 227–229.

Schunkert, H., König, I.R., Kathiresan, S., Reilly, M.P., Assimes, T.L., Holm, H., Preuss, M., Stewart, A.F.R., Barbalic, M., Gieger, C., et al. (2011). Large-scale association analysis identifies 13 new susceptibility loci for coronary artery disease. Nat. Genet. *43*, 333–338.

Shankman, L.S., Gomez, D., Cherepanova, O.A., Salmon, M., Alencar, G.F., Haskins, R.M., Swiatlowska, P., Newman, A.A.C., Greene, E.S., Straub, A.C., et al. (2015). KLF4-dependent phenotypic modulation of smooth muscle cells has a key role in atherosclerotic plaque pathogenesis. Nat. Med. *21*, 628–637.

Sheikh, A.Q., Lighthouse, J.K., and Greif, D.M. (2014). Recapitulation of Developing Artery Muscularization in Pulmonary Hypertension. Cell Rep. *6*, 809–817.

Shi, N., Mei, X., and Chen, S.-Y. (2019). Smooth Muscle Cells in Vascular Remodeling.

Arterioscler. Thromb. Vasc. Biol. *39*.

Shikatani, E.A., Chandy, M., Besla, R., Li, C.C., Momen, A., El-Mounayri, O., Robbins, C.S., and Husain, M. (2016). c-Myb Regulates Proliferation and Differentiation of Adventitial Sca1+ Vascular Smooth Muscle Cell Progenitors by Transactivation of Myocardin. Arterioscler. Thromb. Vasc. Biol. *36*, 1367–1376.

Sinha, S., Iyer, D., and Granata, A. (2014). Embryonic origins of human vascular smooth muscle cells: implications for in vitro modeling and clinical application. Cell. Mol. Life Sci. *71*, 2271–2288.

Skelly, C.L., Chandiwal, A., Vosicky, J.E., Weichselbaum, R.R., and Roizman, B. (2007). Attenuated herpes simplex virus 1 blocks arterial apoptosis and intimal hyperplasia induced by balloon angioplasty and reduced blood flow.

Souilhol, C., Harmsen, M.C., Evans, P.C., and Krenning, G. (2018). Endothelial–mesenchymal transition in atherosclerosis. Cardiovasc. Res. *114*, 565–577.

Tang, J., Wang, H., Huang, X., Li, F., Zhu, H., Li, Y., He, L., Zhang, H., Pu, W., Liu, K., et al. (2020). Arterial Sca1+ Vascular Stem Cells Generate De Novo Smooth Muscle for Artery Repair and Regeneration. Cell Stem Cell *26*, 81-96.e4.

Tang, Z., Wang, A., Yuan, F., Yan, Z., Liu, B., Chu, J.S., Helms, J.A., and Li, S. (2012). Differentiation of multipotent vascular stem cells contributes to vascular diseases. Nat. Commun. *3*, 875.

Tang, Z., Wang, A., Wang, D., and Li, S. (2013). Smooth muscle cells: to be or not to be? Response to Nguyen et Al. Circ. Res. *112*, 23–26.

Tobin, S.W., Li, S.-H., Li, J., Wu, J., Yeganeh, A., Yu, P., Weisel, R.D., and Li, R.-K. (2017). Dual roles for bone marrow–derived Sca-1 cells in cardiac function. FASEB J. *31*, 2905–2915.

Tsai, T.-N., Kirton, J.P., Campagnolo, P., Zhang, L., Xiao, Q., Zhang, Z., Wang, W., Hu, Y., and Xu, Q. (2012). Contribution of stem cells to neointimal formation of decellularized vessel grafts in a novel mouse model. Am. J. Pathol. *181*, 362–373.

Vallier, L., Touboul, T., Brown, S., Cho, C., Bilican, B., Alexander, M., Cedervall, J., Chandran, S.,

Ährlund-Richter, L., Weber, A., et al. (2009). Signaling Pathways Controlling Pluripotency and Early Cell Fate Decisions of Human Induced Pluripotent Stem Cells. Stem Cells *27*, 2655–2666.

Wan, M., Li, C., Zhen, G., Jiao, K., He, W., Jia, X., Wang, W., Shi, C., Xing, Q., Chen, Y.-F., et al. (2012). Injury-activated transforming growth factor β controls mobilization of mesenchymal stem cells for tissue remodeling. Stem Cells *30*, 2498–2511.

Wang, G., Zhang, Z., Xu, Z., Yin, H., Bai, L., Ma, Z., Decoster, M.A., Qian, G., and Wu, G. (2010). Activation of the sonic hedgehog signaling controls human pulmonary arterial smooth muscle cell proliferation in response to hypoxia. Biochim. Biophys. Acta *1803*, 1359–1367.

Wang, Y.-L., Liu, L.-Z., He, Z.-H., Ding, K.-H., and Xue, F. (2012). Phenotypic transformation and migration of adventitial cells following angioplasty. Exp. Ther. Med. *4*, 26–32.

Wong, L.C.Y., and Langille, B.L. (1996). Developmental Remodeling of the Internal Elastic Lamina of Rabbit Arteries. Circ. Res. *78*, 799–805.

Wu, Y., Liu, X., Guo, L.-Y., Zhang, L., Zheng, F., Li, S., Li, X.-Y., Yuan, Y., Liu, Y., Yan, Y.-W., et al. (2019). S100B is required for maintaining an intermediate state with double-positive Sca-1+ progenitor and vascular smooth muscle cells during neointimal formation. Stem Cell Res. Ther. *10*, 294.

Yuan, F., Wang, D., Xu, K., Wang, J., Zhang, Z., Yang, L., Yang, G.-Y., and Li, S. (2017). Contribution of Vascular Cells to Neointimal Formation. PLoS One *12*, e0168914.

Zhang, C., Zeng, L., Emanueli, C., and Xu, Q. (2013). Blood flow and stem cells in vascular disease. Cardiovasc. Res. *99*, 251–259.

Zhang, L., Issa Bhaloo, S., Chen, T., Zhou, B., and Xu, Q. (2018). Role of Resident Stem Cells in Vessel Formation and Arteriosclerosis. Circ. Res. *122*, 1608–1624.

Zhang, Y., Mu, Q., Zhou, Z., Song, H., Zhang, Y., Wu, F., Jiang, M., Wang, F., Zhang, W., Li, L., et al. (2016). Protective effect of irisin on atherosclerosis via suppressing oxidized low density lipoprotein induced vascular inflammation and endothelial dysfunction. PLoS One *11*.

Zhou, S., Zhu, W., Zhang, Y., Pan, S., and Bao, J. (2018). S100B promotes microglia M1 polarization and migration to aggravate cerebral ischemia. Inflamm. Res. *67*, 937–949.

Figure 1

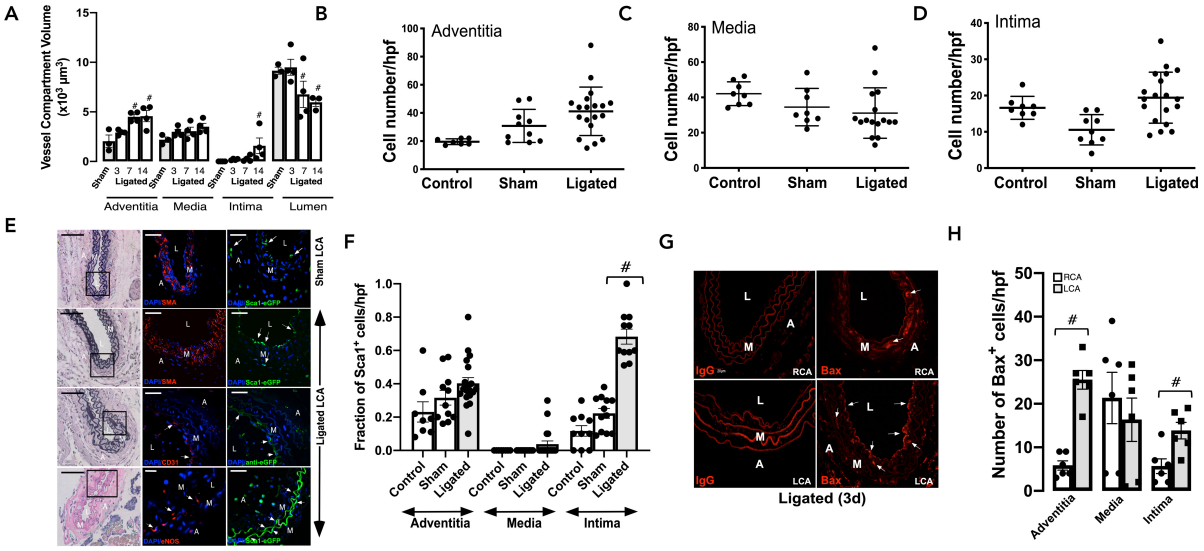
A
Vessel Compartment Volume (x10³ µm³)
Sham
3 7 14
Ligated
Adventitia
Media
Intima
Lumen
B
Adventitia
Cell number/hpf
Control
Sham
Ligated
C
Media
D
Intima
E
Sham LCA
Ligated LCA
F
Fraction of Sca1⁺ cells/hpf
G
IgG
Bax
RCA
LCA
Ligated (3d)
H
Number of Bax⁺ cells/hpf
RCA
LCA

Figure 2

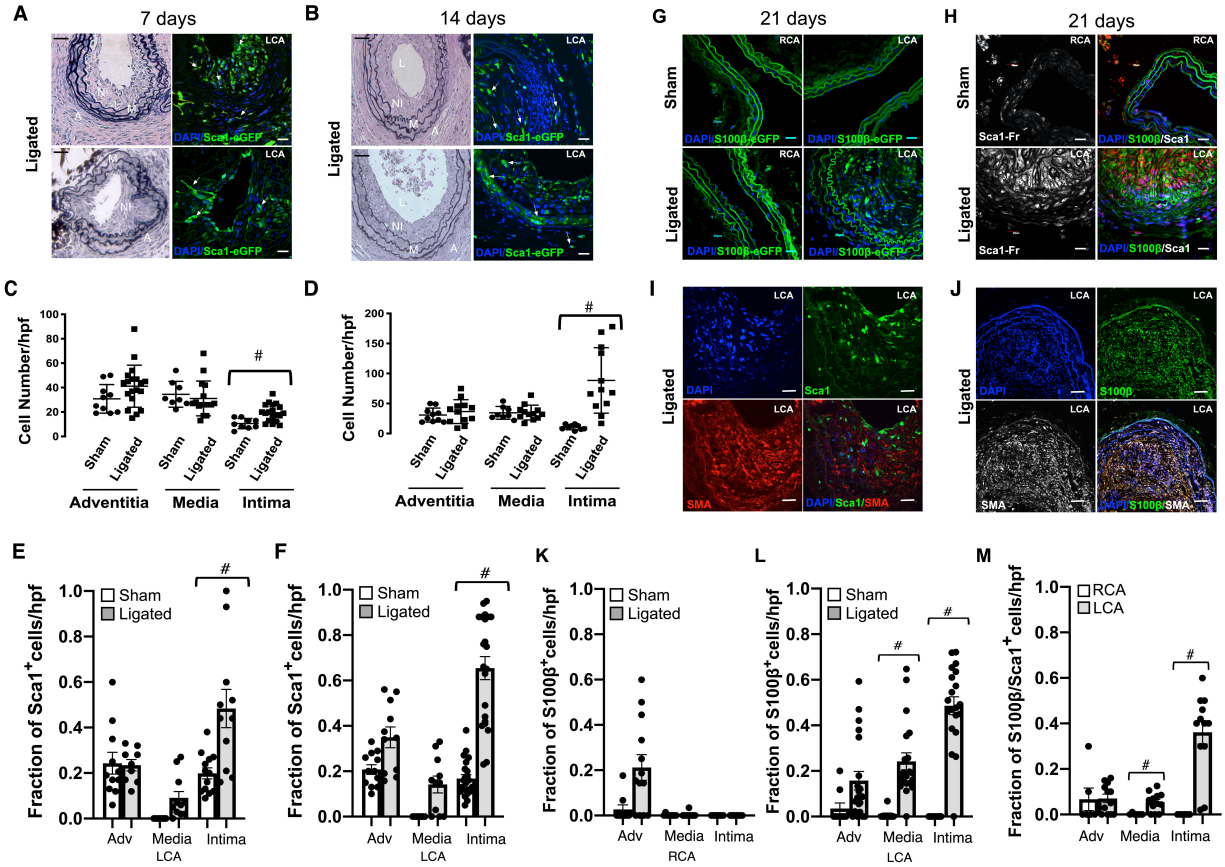
A
7 days
B
14 days
G
21 days
H
21 days
Ligated
Sham
LCA
RCA
DAPI/Sca1-eGFP
DAPI/S100β-eGFP
Sca1-Fr
DAPI/S100β/Sca1
C
D
Cell Number/hpf
Sham
Ligated
Adventitia
Media
Intima
I
J
DAPI
Sca1
S100β
SMA
DAPI/Sca1/SMA
DAPI/S100β/SMA
E
F
K
L
M
Fraction of Sca1+cells/hpf
Fraction of S100β+cells/hpf
Fraction of S100β/Sca1+cells/hpf
Adv
Media
Intima
RCA
LCA
#

Figure 3

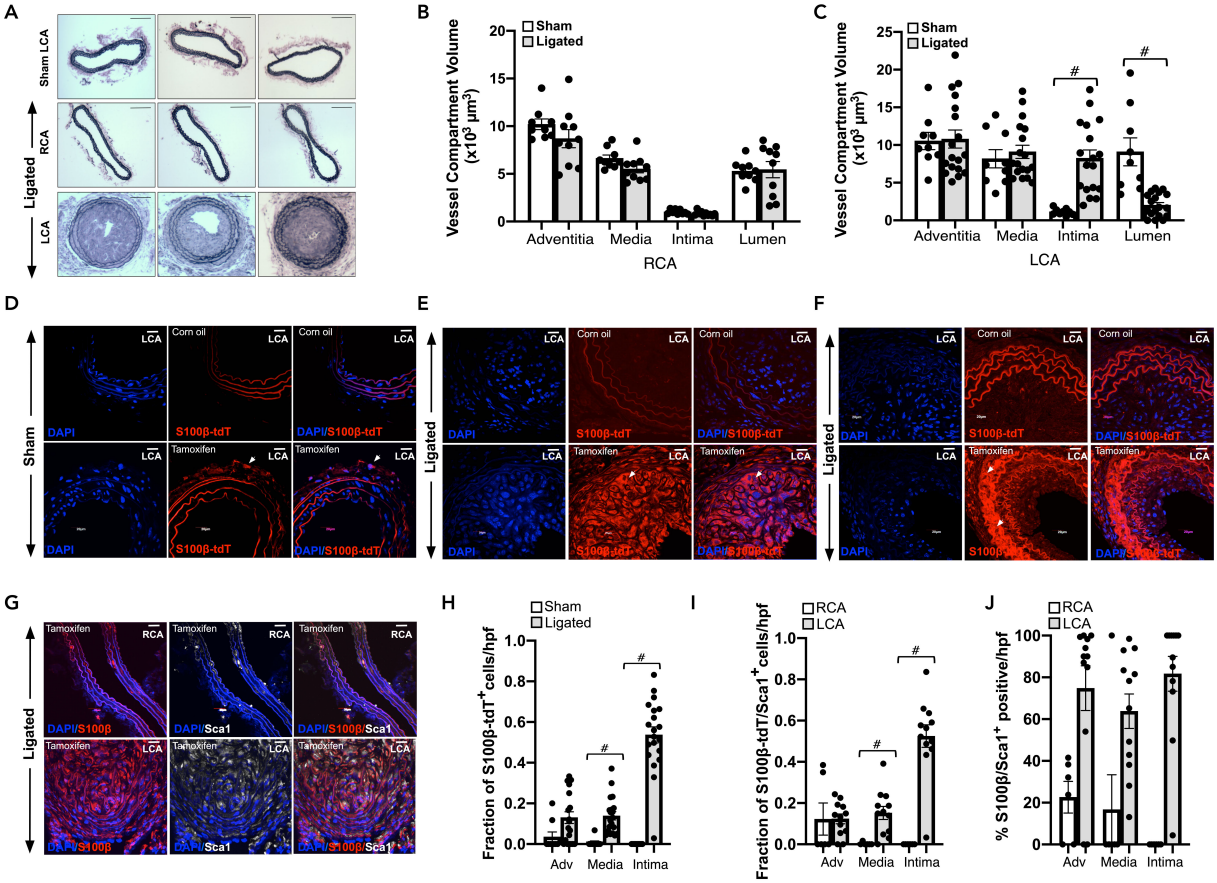
A
Sham LCA
Ligated
RCA
LCA
B
Sham
Ligated
Vessel Compartment Volume (x10³ µm³)
Adventitia
Media
Intima
Lumen
RCA
C
Sham
Ligated
Vessel Compartment Volume (x10³ µm³)
Adventitia
Media
Intima
Lumen
LCA
D
Sham
Corn oil
Tamoxifen
LCA
DAPI
S100β-tdT
DAPI/S100β-tdT
E
Ligated
Corn oil
Tamoxifen
LCA
DAPI
S100β-tdT
DAPI/S100β-tdT
F
Ligated
Corn oil
Tamoxifen
LCA
DAPI
S100β-tdT
DAPI/S100β-tdT
G
Ligated
Tamoxifen
RCA
LCA
DAPI/S100β
DAPI/Sca1
DAPI/S100β/Sca1
H
Sham
Ligated
Fraction of S100β-tdT+ cells/hpf
Adv
Media
Intima
I
RCA
LCA
Fraction of S100β-tdT/Sca1+ cells/hpf
Adv
Media
Intima
J
RCA
LCA
% S100β/Sca1+ positive/hpf
Adv
Media
Intima

Figure 4

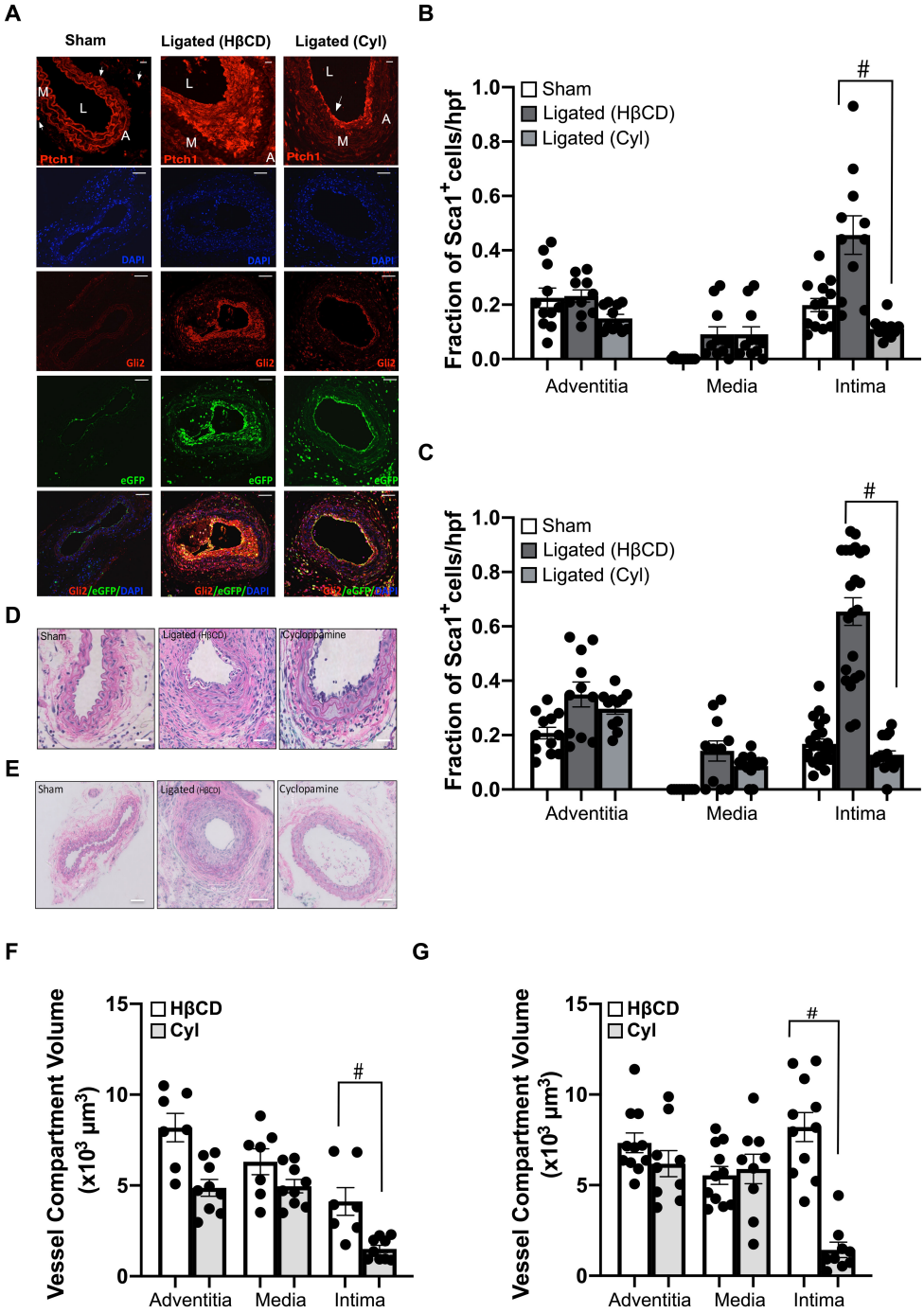
A
Sham
Ligated (HβCD)
Ligated (Cyl)
Ptch1
DAPI
Gli2
eGFP
Gli2/eGFP/DAPI
B
Fraction of Sca1+cells/hpf
Sham
Ligated (HβCD)
Ligated (Cyl)
Adventitia
Media
Intima
#
C
Fraction of Sca1+cells/hpf
Sham
Ligated (HβCD)
Ligated (Cyl)
Adventitia
Media
Intima
#
D
Sham
Ligated (HβCD)
Cyclopamine
E
Sham
Ligated (HβCD)
Cyclopamine
F
Vessel Compartment Volume (x10³ µm³)
HβCD
Cyl
Adventitia
Media
Intima
#
G
Vessel Compartment Volume (x10³ µm³)
HβCD
Cyl
Adventitia
Media
Intima
#

Figure 5

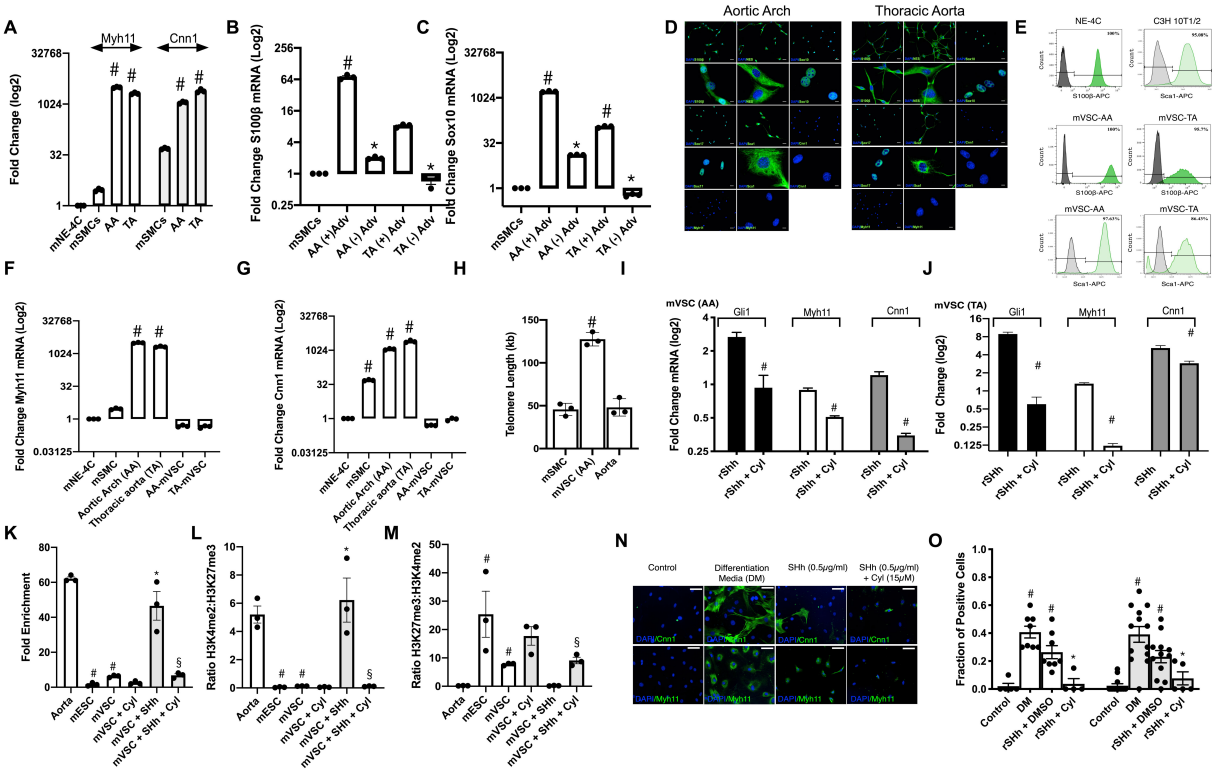
A
Myh11
Cnn1
Fold Change (log2)
mNE-4C
mSMCs
AA
TA
B
Fold Change S100β mRNA (Log2)
AA (+) Adv
AA (-) Adv
TA (+) Adv
TA (-) Adv
C
Fold Change Sox10 mRNA (Log2)
D
Aortic Arch
Thoracic Aorta
E
NE-4C
C3H 10T1/2
mVSC-AA
mVSC-TA
S100β-APC
Sca1-APC
F
Fold Change Myh11 mRNA (Log2)
Aortic Arch (AA)
Thoracic aorta (TA)
AA-mVSC
TA-mVSC
G
Fold Change Cnn1 mRNA (Log2)
H
Telomere Length (kb)
mSMC
mVSC (AA)
Aorta
I
mVSC (AA)
Gli1
Fold Change mRNA (log2)
rShh
rShh + Cyl
J
mVSC (TA)
Fold Change (log2)
K
Fold Enrichment
Aorta
mESC
mVSC
mVSC + Cyl
mVSC + SHh
mVSC + SHh + Cyl
L
Ratio H3K4me2:H3K27me3
M
Ratio H3K27me3:H3K4me2
N
Control
Differentiation Media (DM)
SHh (0.5μg/ml)
SHh (0.5μg/ml) + Cyl (15μM)
DAPI/Cnn1
DAPI/Myh11
O
Fraction of Positive Cells
Control
DM
rSHh + DMSO
rSHh + Cyl

Figure 6

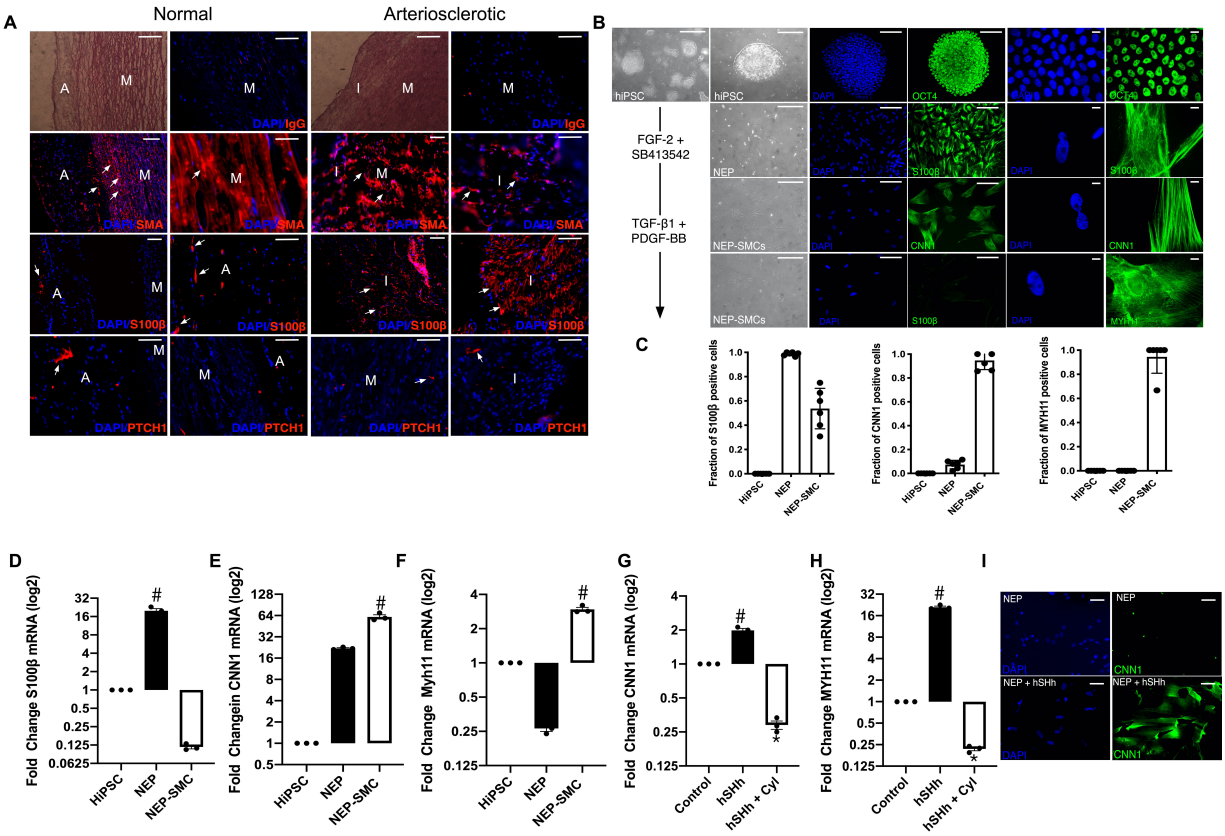
A
Normal
Arteriosclerotic
DAPI/IgG
DAPI/SMA
DAPI/S100β
DAPI/PTCH1
B
hiPSC
OCT4
FGF-2 +
SB413542
NEP
S100β
TGF-β1 +
PDGF-BB
NEP-SMCs
CNN1
MYH11
C
Fraction of S100β positive cells
Fraction of CNN1 positive cells
Fraction of MYH11 positive cells
HiPSC
NEP
NEP-SMC
D
Fold Change S100β mRNA (log2)
E
Changein CNN1 mRNA (log2)
F
Fold Change Myh11 mRNA (log2)
G
Fold Change CNN1 mRNA (log2)
Control
hSHh
hSHh + Cyl
H
Fold Change MYH11 mRNA (log2)
I
NEP + hSHh

Supplementary Table I

Antibodies and their corresponding dilutions used in immunohistochemistry.

Antibody/Product Name	Supplier/Product Number	Dilutions
Rat anti-mouse Sca1/Ly6A/E antibody [D7] (FITC) antibody	Abcam (ab25031)	1/200
Rabbit anti-mouse/rat alpha smooth muscle cell α-actin antibody	Abcam (ab5694)	1/200
Anti-Patched / PTCH1 antibody, Mouse monoclonal	Abcam (Ab55629)	1/100
Anti-Actin, α-Smooth Muscle antibody, Mouse monoclonal	Sigma (A5228)	1/200
Anti-S100-β (CT) Antibody, clone EP1576Y, rabbit monoclonal	Millipore (04-1054)	1/100
Chicken anti-GFP antibody	Abcam (ab13970)	1/1000
Rabbit Anti-RFP/dT antibody	Abcam (ab62341)	1/1000

Supplementary Table II

Antibodies and their corresponding dilutions used in immunocytochemistry/western blot.

Antibody/Product Name	Supplier/Product Number	Dilutions
Mouse anti-mouse/rat nestin [Rat-401]	Abcam (ab11306)	1/200
Rabbit anti-mouse Calponin [EP798Y]	Abcam (ab46794)	1/200
Goat anti-mouse/rat/human smooth muscle Myosin heavy chain	Santa Cruz (sc-79079)	1/200
Mouse anti-human/rat SOX10	R&D System (MAB2864)	1/100
Mouse anti-human SOX17	R&D System (MAB1924)	1/100
Rabbit Anti-S100β	Merck Millipore (ABN59)	1/100
Rabbit Anti-mouse/rat S100β [EP1576Y]	Abcam (ab52642)	1/100
Rabbit anti-mouse/rat Sca1	Millipore (AB4336)	1/100

Alexa Fluor® 488 Goat anti-mouse IgG	Invitrogen (A-11001)	1/1000
Alexa Fluor® 488 Goat anti-rabbit IgG	Invitrogen (A-11008)	1/1000
Alexa Fluor® 488 Donkey anti-goat IgG	Invitrogen (A-11055)	1/1000

Supplementary Table III

Antibodies used in Chromatin Immunoprecipitation (ChIP)

Antibody/Product Name	Supplier/Product Number
Rabbit anti-mouse Tri-Methyl-Histone H3 (Lys27) [C36B11]	Cell Signalling Technology (9733S)
Rabbit anti-mouse Di-Methyl-Histone H3 (Lys4) [C64G9]	Cell Signalling Technology (9725S)
Normal Rabbit IgG (ChIP graded)	Cell Signalling Technology (2729)

Supplementary Table IV

Customised primers used in this study from Integrity DNA Technology (IDT).

Customised primer		Sequences
Mm_Sm-mhc (Myh11)	Forward	5' - GCA GTG AGC TCT CAG TCA TC - 3’
	Reverse	5' - CAA TGC CTC CTC TGA CAA GT - 3'
Mm_Cnn1	Forward	5’ - GCT TGT CTG CTG AAG TAA AGA AC - 3'
	Reverse	5’ - TCC ATG AAG TTG TTC CCG ATG - 3'
Mm_Gli1	Forward	5' - TTG GAT TGA ACA TGG CGT CT - 3'
	Reverse	5' - CCT TTC TTG AGG TTG GGA TGA - 3'
Mm_Hprt	Forward	5’ - GGC TAT AAG TTC TTT GCT GAC CTG C - 3'
	Reverse	5’ - GCT TGC AAC CTT AAC CAT TTT GGG - 3'
Mm_Gaphd	Forward	5’ - GCC TCC AAG GAG TAA GAA AC - 3'
	Reverse	5’ - GCC TCC AAG GAG TAA GAA AC - 3'
	Forward	5’ - CCC TCC CTT TGC TAA ACA CA - 3'

Mm_ Sm-mhc (Myh11) for ChIP PCR	Reverse	5’ - CCA GAT CCT GGG TCC TTA CA - 3'

Primers used in this study from QIAGEN.

Primer	Product Name	Product Code
mHprt-1	Mm_Hprt_1_SG QuantiTect Primer Assay	QT00166768
mS100β	Mm_S100β_1_SG QuantiTect Primer Assay	QT00151536
mSox10	Mm_Sox10_1_SG QuantiTect Primer Assay	QT00295204
mNestin	Mm_Nes_1_SG QuantiTect Primer Assay	QT00316799
mGapdh	Mm_Gapdh_3_SG QuantiTect Primer Assay	QT01658692
mPax6	Mm_Pax6_1_SG QuantiTect Primer Assay	QT01052786
mPax1	Mm_Pax1_1_SG QuantiTect Primer Assay	QT01052779
mKdr	Mm_Kdr_1_SG QuantiTect Primer Assay	QT00097020
mTbx6	Mm_Tbx6_1_SG QuantiTect Primer Assay	QT00098861
hCNN1	Hs_CNN1_1_SG_QuantiTech Primer	QT00067718
hHPRT1	Hs_HPRT1_1_SG QuantiTect Primer	QT00059066
hMYH11	Hs_MYH11_1_SG QuantiTech Primer	QT00069391
hS100β	Hs_S100B_1_SG QuantiTect Primer Assay	QT00059164
rCnn1	Rn_Cnn1_1_SG QuantiTect Primer	QT01081115
rGli1	Rn_Gli1_1_SG QuantiTect Primer	QT01290324
rGapdh	Rn_Gapd_1_SG QuantiTect Primer	QT00199633
rHprt-1	Rn_Hprt1_1_SG QuantiTect Primer	QT00199640

Supplementary Table V

Antibodies and their corresponding dilutions used in Flow Cytometry.

Antibody/Product Name	Supplier/Product Number	Dilutions
Rat anti-mouse Sca1 (Ly-6A/E) [E13-161.7]	STEMCELL Technology (60032)	1/100

Rat anti-mouse IgG2a, kappa Isotype [RTK2758]	STEMCELL Technology (60076)	1/100
Rabbit Anti-mouse/rat S100β [EP1576Y]	Abcam (ab52642)	1/100
Normal Rabbit IgG (F graded)	Cell Signalling Technology (2729)	1/100
Rabbit-IgG Alexa-Fluor 488, Isotype Ctl	Bioss (bs-0295p-A488)	1/100
FITC Rat IgG2a, κ Isotype Control	BioLegend (400505)	1/100
PE Rat IgG2a, κ Isotype Control	MSC (400507)	1/100
Anti-Mouse Sca1	Miltenyi Biotech (130-093-222)	1/100
Anti-Mouse Sca1 Antibody, Clone	STEMCELL (E13-161.7 60032)	1/100
Monoclonal anti-Nestin Clone 10C2 Mouse IgG	ThermoScientific (MA1-110)	1/100
Polyclonal Rabbit anti-Pax6	Abcam (Ab5790)	1/100
Monoclonal Rabbit anti-Sox10 Clone EPR4007 Rabbit IgG	Abcam (Ab155279)	1/100
Polyclonal Rabbit anti-Sox17	Millipore (09-038)	1/100
Monoclonal Rabbit S100β Clone EP1576Y	Millipore (04-1054)	1/100
Polyclonal Rabbit Pax 6	Abcam (Ab5790)	1/100
SMA Mouse Monoclonal Clone 1A4	Sigma (A2547)	1/100
Cnn1 1 Mouse Monoclonal Clone hCP	Sigma (C2687)	1/100
Myh11 Mouse Monoclonal Clone 1G12	Abcam (Ab683)	1/100
Alexa Fluor 546 Goat anti-rabbit (H+L)	Life Technologies (A-11035)	1/100
Alexa Fluor 546 Goat anti-mouse (H+L)	Life Technologies (A-11030)	1/100
Alexa Fluor 488 Goat anti-rabbit (H+L)	Life Technologies (A-11008)	1/100
Alexa Fluor 488 Goat anti-mouse (H+L)	Life Technologies (A-11001)	1/100
Alexa Fluor 488 Donkey anti-goat (H+L)	Life Technologies (A-110055)	1/100

Supplementary Figures

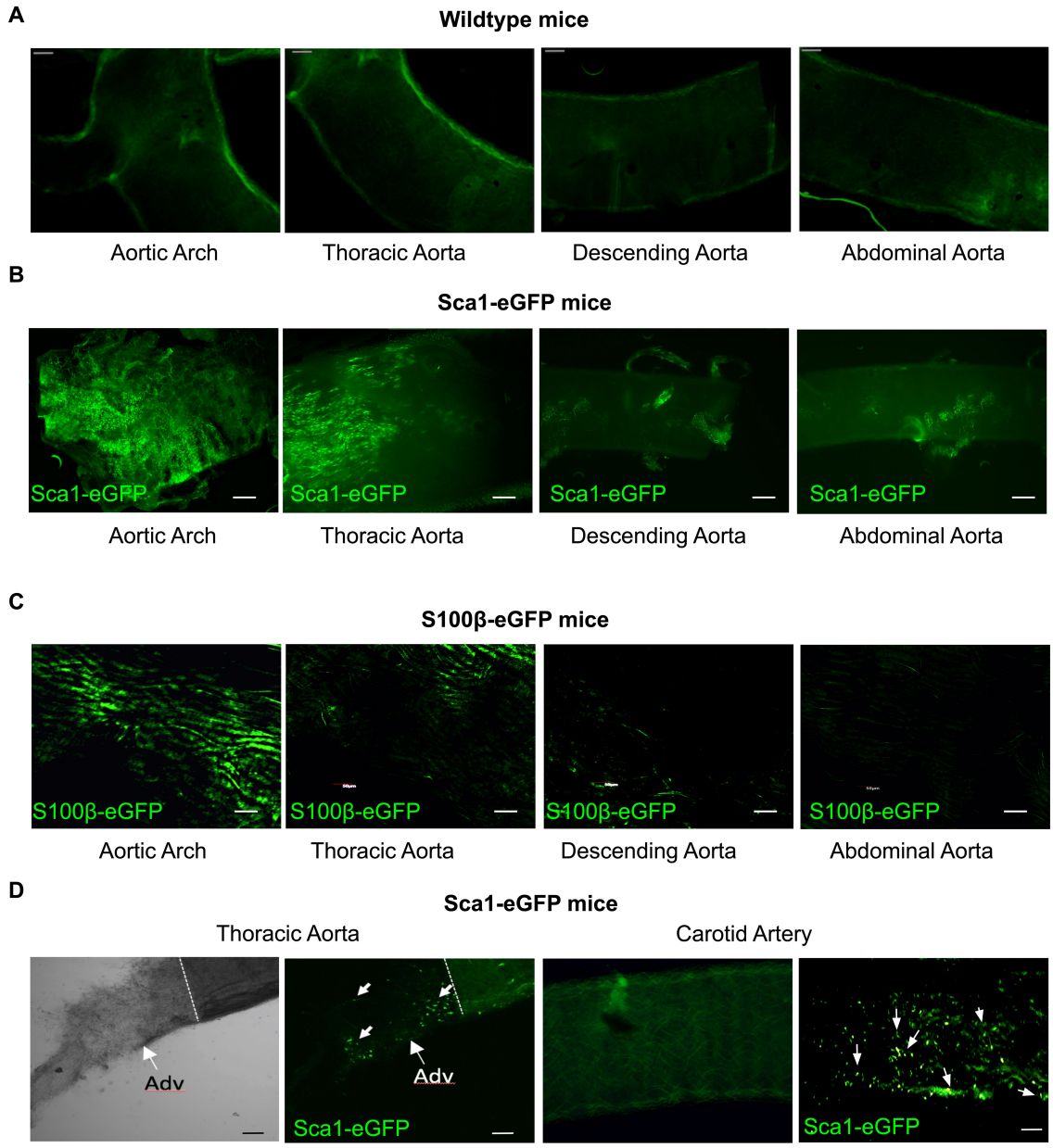

Figure S1 (related to Figure 1 and 2). Sca1 and S100β cells are present in perivascular regions of murine arteries. **A-C.** Whole mount analysis of wildtype control**,** Sca1-eGFP expression and S100β-eGFP expression in aortic arch, thoracic aorta, descending aorta and abdominal aorta. **D.** Sca1-eGFP expression in mouse aorta following removal of the aortic media (dashed line) and in carotid artery of Sca1-eGFP transgenic mice. Each image is representative of 5 images from 3 animals

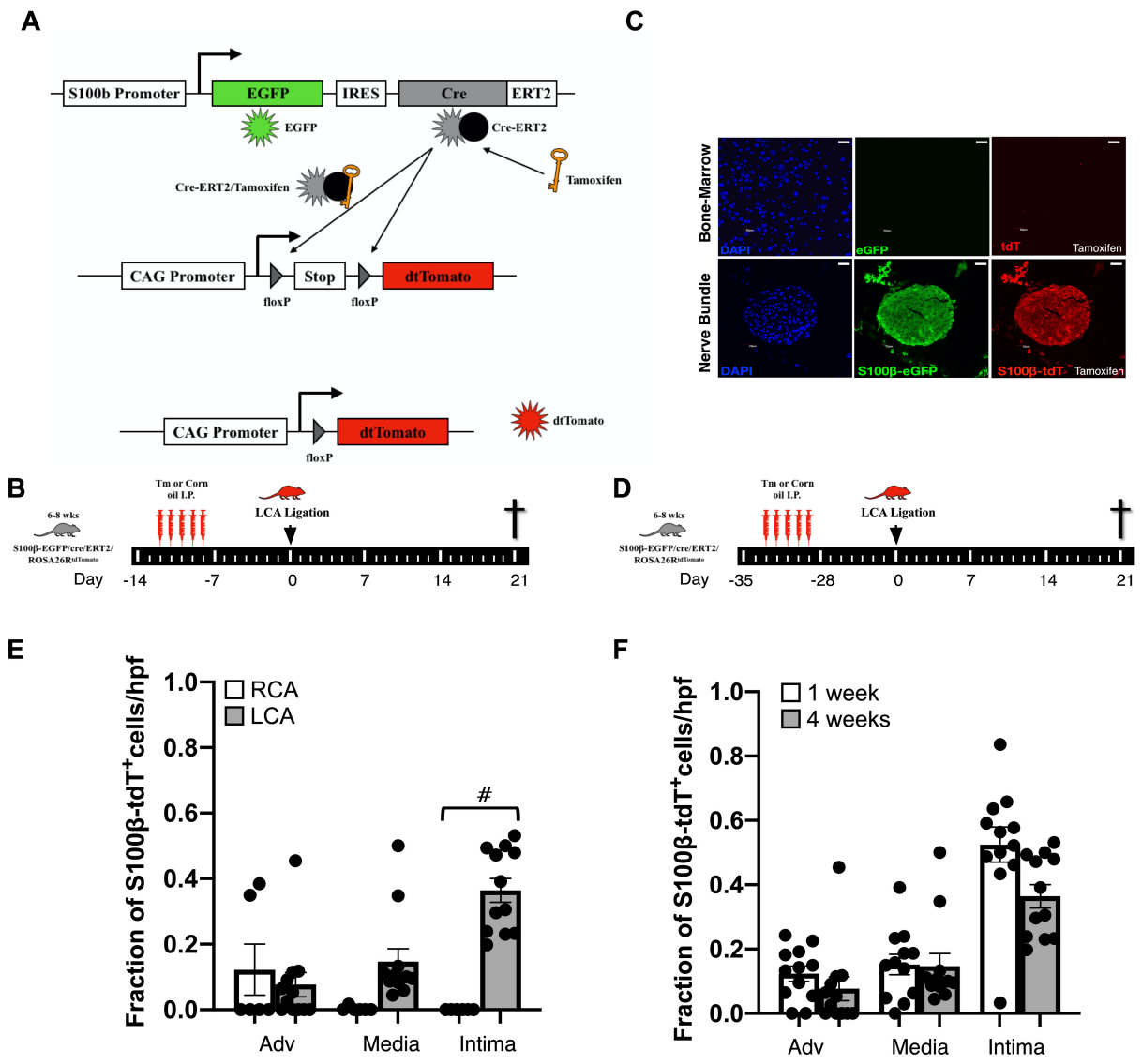

Figure S2 (related to Figure 3) A. Schematic diagram showing generation of S100β-CreERT2-Rosa26-tdTomato. **B**. Tm protocol of 1 week washout prior to ligation. **C.** Representative confocal fluorescence images of S100β-tdT expression in bone marrow smears and herrings nerve bundle in S100β-CreERT2-Rosa26-tdTomato **D.** Tm protocol of 4 week washout prior to ligation. **E.** The fraction of S100β-tdT cells within the adventitial, medial, intimal layers of LCA compared to RCA after 4 week washout. **F.** Comparison of the fraction of S100β-tdT cells within the adventitial, medial, intimal layers of LCA between 1 week and 4 week Tm washout protocols. Data are the mean ± SEM of 3-5 representative images from 3 animals, #p<0.05 vs RCA controls.

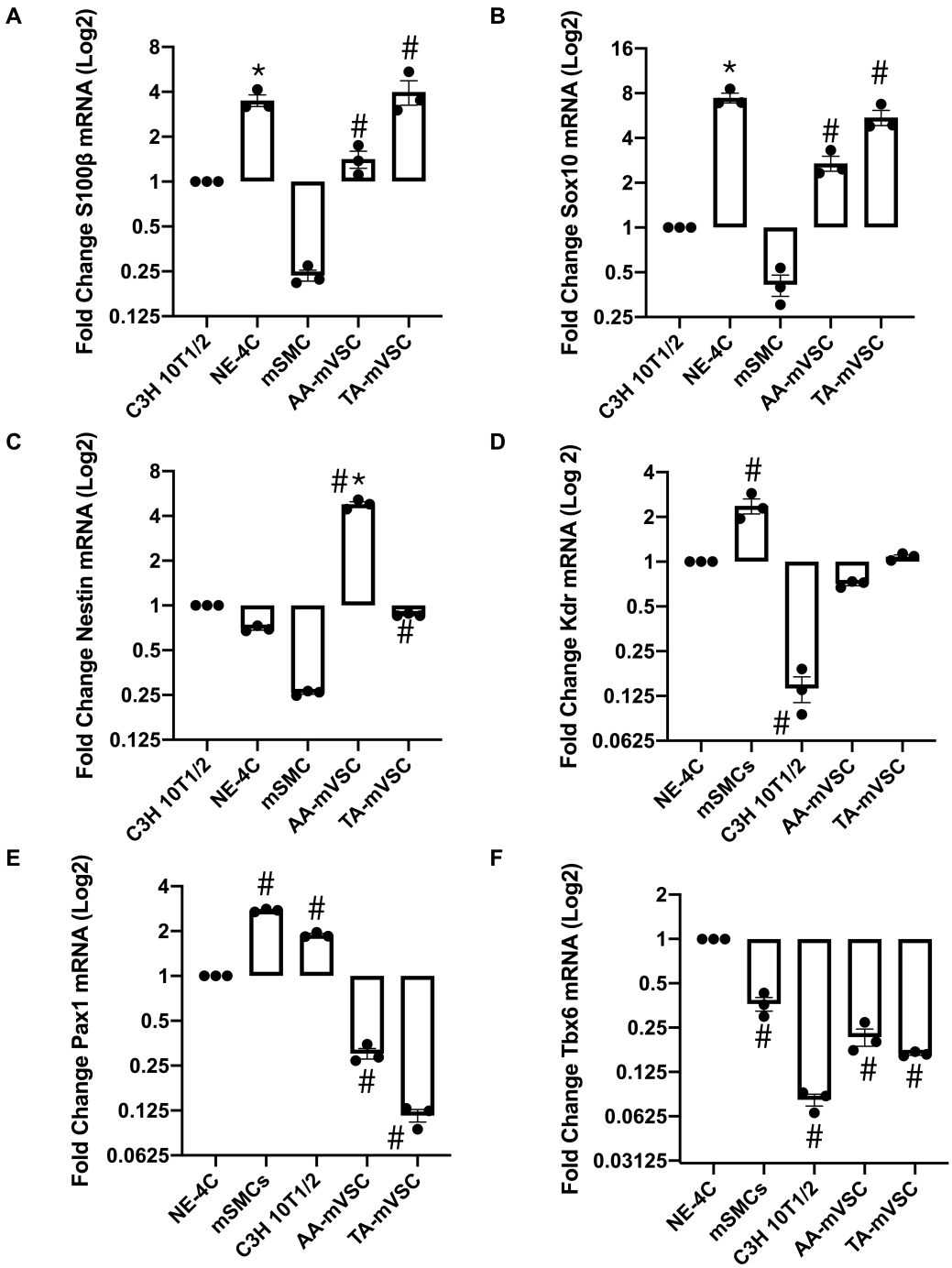

Figure S3 (related to Figure 5). A-C. Relative levels of neuroectoderm markers (S100β, Sox10 and Nestin) and **D-F.** paraxial mesoderm markers (Kdr, Pax1 and Tbx6) in vSCs isolated from AA and TA regions of the mouse aorta. Data are expressed as the Log2 fold change in mRNA levels relative to C3H 10T1/2 cells or neural stem cells (NE-4C) in culture and are the mean ± SEM of 3 independent cultures, *p≤ 0.05 vs C3H 10T1/2 cells (A-C), #p≤ 0.05 vs NE-4C (D-F).